Student thesis series INES nr 648

Applying BROOK90 to model the Water Balance of the spruce forest in Hyltemossa, Sweden

Nele Noack

2024
Department of
Physical Geography and Ecosystem Science
Lund University
Sölvegatan 12
S-223 62 Lund
Sweden

Nele Noack (2024).
Applying BROOK90 to model the Water Balance of the spruce forest in Hyltemossa, Sweden (English)
Bachelor's degree thesis, 15 credits in Physical Geography and Ecosystem Science
Department of Physical Geography and Ecosystem Science, Lund University

Level: Bachelor of Science (BSc)

Course duration: *March* 2024 until *June* 2024

Disclaimer

Applying BROOK90 to model the Water Balance of the spruce forest in Hyltemossa, Sweden

---

Nele Noack

Bachelor thesis, 15 credits, in Physical Geography and Ecosystem Science

Thomas Holst
Department of Physical Geography and Ecosystem Science, Lund University

Exam committee:
Harry Lankreijer,
Department of Physical Geography and Ecosystem Science, Lund University

Tobias Biermann,
Department of Physical Geography and Ecosystem Science, Lund University

Acknowledgements

I would like to express my gratitude to my supervisor for his valuable guidance and help during this thesis. Many thanks to my examiners Harry Lankreijer and Tobias Biermann as well as my opposition Martin Weibull and Migle Stogeviciute for helpful insights. Thanks should also go to Lund University and the Department of Physical Geography and Ecosystem Science for this opportunity. Lastly, I would like to thank my friends and family for support during this time.

Abstract

This thesis evaluated the performance of the water balance model BROOK90 for an even aged spruce forest in southern Sweden. The water balance of the forest was modelled from 1950 onwards to find periods and patterns of drought. Moreover, the impact of climate change as well as thinning as a strategy to reduce drought stress on the water balance were evaluated. Hyltemossa, a managed Norway spruce forest in southern Sweden and site of a combined ecosystem and atmospheric measurement station by ICOS was chosen as the study site. Using measurement data from ICOS the BROOK90 model was parameterized and validated for the period of 2018 to 2024. The model was then applied with input data from nearby SMHI stations for the period of 1950 to 2024 and drought periods were identified based on the transpiration index and number of dry days. Lastly, stand management, assuming changes in stand density as well as a climate change scenario were applied, by changing the LAI or input data. The results show a robust performance from the BROOK90 model, with the modelled evapotranspiration rate (ET) and soil water content (SWC) not differing significantly from the measurements (R^2 of 0.74 and around 0.97 respectively). Although the model performance varied seasonally, the ET rate and SWC were on average overestimated by the model. Furthermore, the years 1951 to 53, 1959, 1972, 1975 to 76, 2016, 2018, 2020 and 2022 were identified as years with high water stress in the spruce forest, with the most pronounced droughts in 1959 and 2018. Thinning (25% decrease in stand density) was modelled to reduce the water stress at the site by up to 5% and shorten the dry period by about 23 days, with the effect being more pronounced for non-drought years. In contrast, the assumed climate change induced temperature increase by 2°C was shown to intensify and prolong water stress by around 29 days.

Table of Contents

1 Introduction

Water stress can limit the growth of trees during growing seasons and can increase their mortality, due to increased vapour pressure deficit and transpiration rates (Allen et al., 2015; Brodribb et al., 2020; Chapin et al., 2011). This in turn results in cavitation of the xylem and stops the water uptake through roots, causing damages or even the death of the plants. Therefore, weather extreme like droughts, defined as a precipitation deficit over the growing season can lead to increased mortality especially in combination with high temperatures (Allen et al., 2015; Brodribb et al., 2020; Chapin et al., 2011). Furthermore, droughts are projected to become longer, hotter and more frequent in the future reportedly increasing the vulnerability and mortality of forests (Allen et al., 2015; Brodribb et al., 2020; Chen et al., 2021; Seneviratne et al., 2012; Trenberth et al., 2003; Trenberth et al., 2014).

In Sweden, about two thirds of the entire country (28 million hectares) is covered by forest and as of 2015 around 10 percent of the country's employment, sales and export are in the forestry sector, making this ecosystem a highly valuable resource (KSLA, 2015; Roberge et al., 2020). The most common tree species are Norway Spruce (*Picea abies*) and Scots Pine (*Pinus sylvestris*) which make up around 40 % and 38% of the forest cover respectively. They are found mostly in monoculture stands and in Sweden the most restricting resources to these forest ecosystems are nutrient availability and water (Alavi, 2002; KSLA, 2015; Roberge et al., 2020).

Even though there was reportedly a wetting trend with increased soil water and precipitation in Sweden since the 1930s, the country has frequently experienced droughts and dry periods from 1950 onward in 1953, 1976, 1988 to 1989, 1992 to 1993, 2003, 2018 and 2022 (Alavi, 2002; Chen et al., 2021; Hanel et al., 2018; Hänsel et al., 2022; Knutzen et al., 2023). The overall wetting trend is projected to prevail with changing climate. However, the rising temperatures will increase vulnerability of forests to droughts and climate change will bring more frequent heat waves in Scandinavia (Seneviratne et al., 2012; Seneviratne, 2023).

One strategy applied in Swedish forestry to elevate water stress as well as improve growth, light and nutrient access, is thinning (Roberge et al., 2020). It is a widespread practice in the even-age management, the most common forestry approach in Sweden, with typically at least one non-commercial and up to three commercial thinning applications within one stand rotation. While the non-commercial application usually serves to improve vitality and regulates species type, stand height and density, commercial thinning is used to increase the stand quality and sell timber (Roberge et al., 2020). Studies performed by Belmonte et al. (2022); Lagergren (2001), Lagergren et al. (2008) and Zanchi et al. (2014) found that thinning generally reduces water use and can furthermore prolong soil water availability and increase transpiration rates during drought conditions in mixed coniferous and pine forests. Moreover, a study by Saksa et al. (2017) suggests that changes in the water balance from thinning are more pronounced in precipitation rich regions, making it a possible practice to reduce water stress and drought impacts in humid regions of Sweden. However, few studies have looked at impact of thinning on water availability of monocultural spruce forests, which are the second most common forests in Sweden (KSLA, 2015; Roberge et al., 2020).

To study the impact of different management strategies on water stress and availability, the most important variables to consider are the transpiration rate and soil moisture (Heim, 2002; Puhlmann et al., 2019). Both can be measured manually, however, this is done with high costs and uncertainty, especially sap flow measurements for transpiration fluxes (Baumgarten et al., 2014).

Therefore, the application of a water balance model provides an appropriate tool to analyse past drought events in a forest and test the influence of thinning and climate change on forest water stress with more detail than drought indices (Wellpott et al., 2005). For this purpose, the deterministic, parameter-rich hydrological model BROOK90 (Federer, 2002; Federer et al., 2003) has shown to provide a good model fit for evapotranspiration, soil moisture and transpiration rates (Baumgarten et al., 2014; Buchtele et al., 1998; Luong et al., 2020; Tahir, 2012; Wellpott et al., 2005). Tahir (2012) gives an example of applying BROOK90 to study different management strategies and climate change conditions in a mixed pine-spruce forest in central Sweden and an even-aged pine forest in Germany showing that thinning can decrease water deficiency. This leaves the question of how well BROOK90 can model the conditions of a monocultural spruce forest in southern Sweden and how the water supply for such a forest changed in the past, partly representing the conditions projected with climate change in more northern regions (Seneviratne et al., 2012; Seneviratne, 2023).

1.1 Aim

The aim of this thesis is to evaluate the accuracy of the BROOK90 model outputs for the spruce forest in Hyltemossa, a site in southern Sweden, based on field measurements for the period of 2018 to 2024. Furthermore, it aims to model changes in the water balance using weather station data from 1950 to identify periods and patterns of water stress and drought for the spruce forest. Finally, the impact of thinning, as a strategy to reduce drought stress, as well as projected increasing temperatures on the water balance will be evaluated by applying different stand density scenarios in the model.

1.2 Research Questions and Hypotheses

This thesis focusses on the following research questions. How well does the model BROOK90 represent the water balance of the spruce forest? How did the forest react to the changing climate conditions since 1950 regarding its water balance? Which management strategy could be applied in the future to reduce the impact of droughts?

1) Given the complexity of the BROOK90 model and the adjustments made to the input parameters to fit the study site conditions a high accuracy of model is expected. Furthermore, Wellpott et al. (2005) and Luong et al. (2020) showed both a high model fit and accuracy for modelled evapotranspiration rate and soil moisture in their respective forest study sites.
2) As mentioned, southern Sweden experienced periods of drought or dryness in 1953, 1976, 1981 - 83, 1988 - 89, 1992 – 93, 2003 and 2018 and these periods are expected to be reflected in the modelled water stress (Actual Transpiration/Potential Transpiration; AT/PT) (Alavi, 2002; Hanel et al., 2018; Hänsel et al., 2022).
3) Furthermore, Sweden has reportedly experienced a wetting trend since the 1930s which is hypothesized to be reflected in trends in soil water content and precipitation for this study site (Chen et al., 2021).
4) Given that an increase in plant mass leads to higher transpiration and interception rates, with slightly lower soil evaporation, an increase of ET and decrease in soil water content is expected with higher stand density as well as increased water stress due to lower water availability (Alavi, 2002; Dingman, 2015; Puhlmann et al., 2019). Vice versa a decrease in

stand density will lead to reduced water stress, due to lower ET and higher water availability. Accordingly, increasing temperatures lead to higher vapour pressure deficit at the stomata and increased photosynthesis, increasing the transpiration rate and therefore would result in higher water stress (Dingman, 2015; Tahir, 2012).

2 Background

2.1 Water Balance in Forests

The water balance is a concept used in hydrological studies to study the in and outflow of water of a defined area (Dingman, 2015). It applies the mass conservation law to water within this area, which is typically a watershed, but it is also applicable on ecosystem or country scales. According to the mass conservation, the incoming water should be equal to the sum of the outgoing water flux and the change in storage. The basic theory here defines the equation:

Equation 1

$$P + GW_{in} = \Delta S + (Q + ET + GW_{out})$$

Where, P is the precipitation, GW is the groundwater in- and outflow (in, out), Q is the stream outflow, S is the storage term (for all types), and ET is the evapotranspiration rate.

Therefore, the water balance of a forest can be split up into the following basic components:

The **evapotranspiration** (ET) of an ecosystem is the sum of all processes that result in water vapour leaving the system (Dingman, 2015). These include **evaporation** from open water, soil and vegetation, sublimation from ice and snow and **transpiration** through the leaf stomata. When looking at the components, **evaporation** depends on the weather conditions, surface conditions and vegetation properties. The precipitation determines the available water while the temperature and humidity give the water vapour pressure deficit and therefore the capacity of the air to take up water. Moreover, the higher the temperature and windspeed and the lower the humidity, the higher the evaporation rate. Moreover, water evaporates more readily open surfaces, with higher interception from vegetation leading to higher rates (Chapin et al., 2011; Dingman, 2015). Similarly, **transpiration**, is determined by weather condition, vegetation properties and soil properties (Chapin et al., 2011; Dingman, 2015). The process involves water uptake by the roots, transport through the vascular system of the plant to the leaf and evaporation through the stomata in exchange for carbon dioxide and oxygen. This means that plant properties determine the rate of water uptake and transpiration which is often defined in models by several resistance terms. These usually include root resistance (how easily water is taken up from the soil), plant resistance (how easily water is transported within a plant), stomata resistance (how open the stomata are as well as the gas exchange rate with respiration and photosynthesis) and lastly aerodynamic resistance outside the leaves. Transpiration varies therefore with root length, plant height, leaf size and type and stand density. Furthermore, the photosynthesis rate is largely dependent on the incoming radiation and temperature. Moreover, the available water depends on the precipitation amount and intensity and soil properties, where soils with high water holding capacity and pore space for root systems enable higher water uptake, while shallow or dense soils largely limit water availability (Chapin et al., 2011; Dingman, 2015).

The **groundwater** term is also mostly dependent on the soil properties as well as the topography and bedrock type which influence the flow density and speed. The same goes for **stream flow**, which depends on the infiltration rate into the soil, the precipitation intensity and input from ground water flow (Dingman, 2015). The **storage** term includes water stored in open water (rivers, lakes, snow, ice), ground water and vegetation. It is often difficult to determine and therefore attempted to minimize in models by choosing large model timeframes or specific period for which the change in storage can be assumed insignificant (Dingman, 2015).

2.2 Water Balance Models

Over time various hydrological models have been developed to study the water balance of a hydrological system (Abdollahi et al., 2019). Depending on the simulation approach, they can be divided into physically based, statistically based, stochastic and conceptual models. Physically based models utilize concepts from basic physics and provide for parameterization based on the site properties (Dingman, 2015). They are typically rather complex and describe processes at comparatively small scales as compared to conceptual models which provide for often simplified parameters at various scales. Moreover, models can be differentiated by their spatial representation, dividing them into lumped or distributed models, where lumped models assume their parameters and input to fit the entire modelled system (e.g., ecosystem or watershed). Distributed models provide for spatial variability, but often apply lumped models to subregions of the system (Dingman, 2015). It is therefore typically sufficient to use a lumped model for mostly homogeneous systems. On a temporal basis, models are further differentiated into steady state, event-based and continuous models. Continuous models are most fitting to model changes over time, while event-based models are typically used to simulate specific responses to singular input values (Dingman, 2015). As the aim of this thesis is to study changes in the water balance of a monocultural spruce forest over time and evaluate management strategies, a physically based, continuous model is most suitable. Therefore, the physically based, lumped, continuous water balance model BROOK90 was chosen (Federer, 2002).

2.3 Drought and Water stress

Droughts are defined as periods with a water deficit for the ecosystems and can be caused by wind, high temperatures or insufficient precipitation (Seneviratne, 2023). The literature defines three types of droughts: *i Agricultural* or *ecological droughts*, focussing on the effects on the biome and limiting ecosystem functions; *ii Hydrological droughts*, describing a shortage in water bodies and reservoirs, and *iii meteorological droughts*, describing a period of unusual lack of precipitation (Seneviratne, 2023).

To assess the impact of water stress and droughts on ecosystems multiple models and indices were developed over time, including the Standard Precipitation Index (SPI) (Mckee et al., 1993), Consecutive Dry Days (CDD) (Lloyd-Hughes & Saunders, 2002), Palmer Drought Severity Index (PSI) (Palmer, 2006) and Standardized Precipitation-Evapotranspiration Index (SPEI) (Vicente-Serrano et al., 2010). However, these generally only display changes in drought conditions, with the SPI and CDD only considering precipitation variation and the PSI and SPEI integrating effects of accumulative forcing and evapotranspiration (ET) to effectively reflect soil moisture droughts (Lloyd-Hughes & Saunders, 2002; Mckee et al., 1993; Palmer, 2006; Seneviratne et al., 2012; Vicente-Serrano et al., 2010). Hammel and Kennel (2001) therefore suggested to evaluate the water stress conditions of forests using the **transpiration index**, which is given by the ratio of actual and potential transpiration. This provides then a measure of water availability specifically for the vegetation (Hammel & Kennel, 2001; Wellpott et al., 2005).

3 Material and Methods

3.1 Study Area

The study area chosen for this thesis was Hyltemossa, a managed spruce forest located in Scania region, southern Sweden around 40 km east of Helsingborg, 50 km north of Lund and 25 km west of Hässleholm (56.09763° N, 13.41897° E; 115 m above sea level) (Heliasz, Mölder, et al., 2024). The site is managed and owned by Gustafsborg Säteri AB (GustafsborgAB, 2024) and accommodates a combined ecosystem and atmosphere station since 2014 run by the Integrated Carbon Observation System (ICOS) partly funded by the Swedish research council and partly by project partners (Levin et al., 2020). The Hyltemossa Research Station (Htm) is distributed over two stands (35 and 40 years old) mostly consisting of Norway Spruce (*Picea abies*, over 99% cover according to Heliasz, Mölder, et al. (2024)) with small fractions of birch (*Betula sp.*) and Scots pine (*Pinus sylvestris*). The vegetation below the canopy is sparse and consists mostly of mosses covering the sandy till soil. This soil consists mainly of glacial sediments and sandy moraines forming a Cambisol with a thin organic horizon, sometimes replaced by Podsol, on acidic intrusion bedrock (SGU, 2024). Ground water is relatively shallow in the area and some areas show groundwater influence in 1 m depth (Heliasz, Mölder, et al., 2024; ICOS). The topography in the area is relatively flat with a change in elevation of 35 m throughout the site (Levin et al., 2020). Hyltemossa has a temperate humid climate (Cfb after Köppen (1900)) with a mean annual precipitation of 707 mm and mean annual temperature of 7.4 °C, based on climate data from the station in Ljungbyhed from 1961 to 1990, and a prevailing wind direction from the West. The closest weather stations from the Swedish Meteorological and Hydrological Institute (SMHI) are located in Ljungbyhed (13 km West of Hyltemossa, shut down in 2001), Klippan (20 km North of Hyltemossa) and Helsingborg (SMHI, 2024).

The managed forest has a turnover rate of 50 years with the forest growing 31 meters in 100 years on average. One stand (number 2320) was planted in 1983 with an initial stand density of 3300 trees per hectare, after storm damage in 1981 and a clear cut in 1982. Following this the spruce forest was cleared in 1998 and 2005 and thinned in 2009 and 2013 (GustafsborgAB, 2016; Heliasz, Mölder, et al., 2024). Similarly, the second stand (number 2341) was clear cut in 1988 and replanted in 1989, cleared in 1998 and 2012 and thinned by 30% in 2015 (GustafsborgAB, 2016). There is little information on the forest management and properties before 1980 provided. Furthermore, ICOS measured a leaf area index (LAI) ranging from 3.9 to 4.9 with an average of 4.4 for the forest since 2018 and a stand height of 16.7 m with a maximum tree height of 26.6 m in 2022 (Heliasz, Mölder, et al., 2024).

3.2 BROOK90

The hydrological model used here is BROOK90 (Version 4.8a) (Federer, 2019), a parameter-rich, deterministic, one-dimensional model originally developed to study vertical soil water movement of forests as well as evapotranspiration in a daily resolution over the whole year (Federer et al., 2003). The model is a lumped model allowing only to model the water balance of a singular point using physically meaningful parameters (Federer, 2002; Federer et al., 2003). In general, the model can be used to investigate evapotranspiration, water budget, soil water movement in typical forest ecosystems or water management strategies for land use practices (Baumgarten et al., 2014; Combalicer et al., 2008; Hammel & Kennel, 2001; Kronenberg et al., 2013; Schmidt-Walter et al.,

2020; Tahir, 2012; Wellpott et al., 2005). It also provides for studies of streamflow generation from various flow path, as well as studies of flash floods or similar phenomena (Luong et al., 2021; Vilhar et al., 2010; Vorobevskii, 2022; Zheng et al., 2021). Furthermore, comparing outputs to simple models can be used to evaluate the performance of those models (Federer et al., 2003).

3.2.1 Input and Output

BROOK90 requires values for daily precipitation (in mm) and maximum and minimum temperatures (in °C). Furthermore, if available total daily solar radiation (MJ/m²), average daily vapour pressure (kPa) and windspeed (m/s) should be included, otherwise averages or default values will be used in the model. If not provided to the model, solar radiation is estimated by the potential insolation on a horizontal surface which is determined by the day of the year (doy) and latitude and corrected for scattering, reflection and absorption with a radiation of ratio of 0.55 (Federer, Revised - April 9, 2021; Holst et al., 2005). The windspeed is assumed to be 3 m/s and the vapour pressure is estimated as the saturation vapour pressure for the minimum daily temperature (Federer, Revised - April 9, 2021).

The model gives a large variety of output values representing water balance components of the site which can be produced in daily, monthly, or yearly resolution. These include evapotranspiration rate (ET in mm/day), the soil water content (SWAT, in mm), interception (mm/day), available water, soil water deficit, actual (AT) and potential transpiration rate (PT in mm/day) and evaporation rate (in mm/day) from different surfaces, as well as water stress given by the transpiration coefficient (STRES given by AT/PT). Furthermore, flow and groundwater properties such as measured and simulated flow, seepage, soil and storm flow, groundwater table, as well as snow fall and rain to snowpack can be modelled, but are not the focus of this thesis and therefore not included here (Federer, 2002).

3.2.2 Processes

The model considers and models the following processes within the hydrological cycle of an ecosystem (described in detail by Federer (2002); Federer et al. (2003)):

Precipitation is either intercepted by or falls through the forest canopy cover. To allow for a precipitation intensity term and reduce daily interception loss from daily precipitation data, BROOK90 loops through an interception model every hour. It assumes a precipitation duration determined by DURATN, centred around noon. Over this period the rain or snow is assumed to occur at a constant rate which allows for part of the interception evaporation to be allocated to the next day. These processes are treated separately for day and nighttime assuming constant rates for interception and evaporation for these periods, respectively. Throughfall can result in infiltration into the first soil layer or deeper by macropore flow or in streamflow through impaction or pipe flow within the soil. The model also allows for streamflow from delayed flow by downslope soil drainage or groundwater storage. Furthermore, snowmelt processes are included with the melting process depending on the degree day factor, including liquid water content and temperature, and are modified according to the LAI. Evapotranspiration (ET) is the sum of evaporation from interception and soil and transpiration from the plant canopy. It is here based on the Penman-Monteith method (Monteith, 1965), which estimates ET as a functions of vapour pressure deficit, available energy canopy resistance and aerodynamic resistance. The canopy or stomatal resistance here as a function of the LAI and incoming shortwave radiation and vapour pressure as input data. This approach is generally regarded as accurate (Wang et al., 2020).

The model further differentiates between rain and snow evaporation. Here, evaporation from interception assumes no canopy resistance and is based on average storm duration, canopy capacity and aerodynamic resistance within and above the canopy dependent on canopy height and LAI. Soil evaporation resistance is dependent on the water potential of the top soil layer (Federer, 2002; Federer et al., 2003). For all those processes, the model separates between day and night-time based on the day of the year (doy).

To estimate potential interception and separate soil evaporation and transpiration the Shuttleworth and Wallace method is applied (Shuttleworth & Wallace, 1985). This assumes a sparse canopy for a single layer sparse canopy and is applied to the first soil layer. The model further differentiates between potential (PT) and actual transpiration (AT) using a method developed by Federer (1979). While PT is determined by aerodynamic resistance and canopy resistance, estimated from maximum leaf conductance, light penetration, temperature and humidity, AT is a reduced PT based on soil water availability. This is determined by the root distribution, soil water potential, critical leaf water potential, and plant and rhizosphere resistance (Federer, 1979). The aerodynamic resistance here is based on the modified method introduced by Shuttleworth and Gurney (1990) and varies with LAI and canopy height. Transpiration rate is defined as the lesser of daily demand by the air and supply rates from the soil. For this, the daily supply is assumed to be constant over the length of a day and depends on the soil water content and the plant water potential as well as the plant storage uptake at the beginning of the day. The demand rate has a diurnal half sine pattern and the daily term is the integral of this relation over the day (Federer, 1982).

For soil water movement, BROOK90 allows for up to 25 layers of adjustable thickness and properties including water content and potential at field capacity, stone content, water content at saturation and hydraulic conductivity. The vertical movement is determined by Darcy's law for saturated and unsaturated flow and the parameterization of matric potential, hydraulic conductivity and soil water content relationships is based on a formulation modified from Clapp and Hornberger (1978). Streamflow from groundwater is set as a fraction of groundwater per day and groundwater influx is from gravity drainage from the lowest soil layer.

The processes are also displayed in the flow chart provided with the model (Federer, 2019):

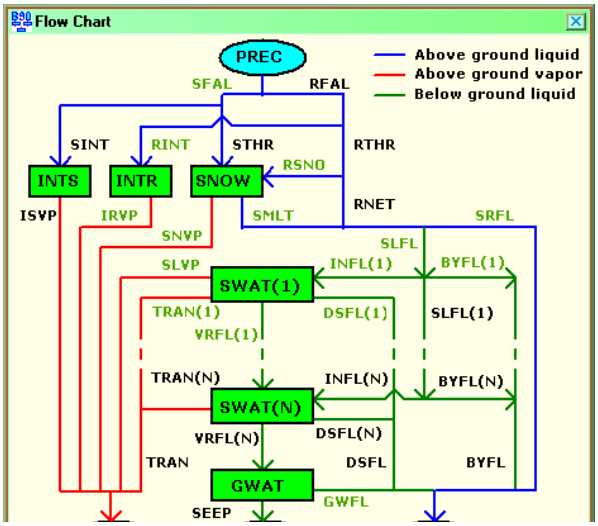

Figure 1: Flowchart showing the water flow paths for the hydrological system modelled in BROOK90 (Federer, 2019). All variables are explained in the following text.

As shown in Figure 1, the incoming precipitation (PRECIP) in the form of snow (SFAL) or rain (RFAL) is either intercepted (INTS, INTR) or falls to the ground as throughfall (THR) where rain either freezes on the snowpack (RSNO) or reaches the soil surface in liquid form together with melted snow (RNET and SMLT). The water then either infiltrates into the soil (SLFL to INFL) or results in surface flow (SRFL) which adds up to complete outflow (FLOW) together with bypass flow (BYFL) and soil out flow (SLFL) from different soil layers (1 to N). The remaining soil water contributes to the soil water table in the form of stored water (SWAT) at different layers which can be taken up by plants for transpiration (TRAN) or in ground water (GWAT determining the seepage SEEP). Intercepted precipitation and transpiration add up to evapotranspiration (EVAP). For further information, detailed processes are described in Federer (2019).

3.2.3 Parameters

BROOK90 utilizes a large variety of physically meaningful parameters, which can be externally altered to fit the specific site and were originally developed for forest sites. However, reasonable results can also be achieved with predetermined parameters, for e.g. spruce forests, described by Federer et al. (2003) (Federer, 2002; Wellpott et al., 2005). All parameters are provided externally in 6 different files: 1) Soil, 2) Flow, 3) Canopy, 4) Location, 5) Fixed and 6) Initial. Important parameters and their value ranges fitted for various ecosystems are described in detail in the model application to allow for reasonable fitting (Federer, 2019).

1) SOIL: The soil file provides properties for a specified number of soil layers (1 to 25) including parameters for layer thickness (THICK, in mm), stone content (STONEF, as fraction), field capacity (water potential PSIF in kPa and volumetric water content THETAF as a fraction), water content at saturation (THSAT, as a fraction), the exponent in the Brooks Corey equation (BEXP), the hydraulic conductivity (KF, in mm/day) and other components of water retention properties of soil layers. While a higher STONEF, with a range of 0 to 1 reduces soil water content (SWC) and evapotranspiration rate (ET), an increased PSIF (b/w -1 and -330kPa) and THETAF (typically 0.1 to 0.5) adds to the ET rate and SWC. The BEXP determines how coarse a soil is (values between 3 and 12) and has low influence on the output with higher BEXP (finer soil) increasing the ET rate and reducing the SWC. Similarly, KF (0.1 to 10 mm/day and typical value of 5 mm/day) shows low influence on the outputs. All these parameters are interconnected.
2) FLOW: The flow file contains parameters describing the infiltration and drainage properties at the location including infiltration depth (IDEPTH, in mm), a parameter determining infiltration distribution throughout the soil profile (INFEXP, with 1 meaning uniform distribution of infiltration and 0 resulting in a wetting front from the first soil level). Other parameters are the fraction of soil that is impermeable (IMPERV, ranging from 0 – fully permeable to 1 - impermeable), parameters for bypass flow and downslope matric flow and drainage out of the soil into groundwater (DRAIN, between 0 – no drainage from the bottom and 1 – vertical drainage by gravity). For this study, bypass flow and downslope matric flow were disregarded, as it does not focus on flow rate and soil properties are mostly unknown for the soil, by setting the respective parameters to “0”. IDEPTH, INFEXP and DRAIN all have low influence on the outputs, while IMPERV impacts the water availability with a higher fraction resulting in reduced ET and increased SWC.
3) CANOPY: The canopy file includes properties of the assumed single layer canopy, which is here a forest canopy, including parameters on external factors, the canopy structure and

photosynthesis processes in the plant. Some of the parameters are the albedo (ALB), maximum tree height (MAXHT, in m) and leaf area index (MAXLAI), a ratio for stem area index to canopy height (CS, typically 0.035). Furthermore, internal conductivity of the plant (MXKPL, typically around 8 mm/ MPa,day) and internal plant resistance (FXYLEM, between 0 and 1) as well as parameters on photosynthetic rate such as maximum leaf conductance for fully open stomata (GLMAX, 0.2 to 2), leaf width (LWIDTH) and radiation extinction (CR) in the canopy can be adjusted. The root density in layers of 100 mm thickness and the overall maximum root length can be changed. The LAI and height can be determined by measurements with an increased LAI usually resulting in higher ET rates. MXKPL shows an increasing ET rate for higher MXKPL and only gradual changes to the SWC. A higher FXYLEM similarly results in increased ET as well as lowered SWC, while the GLMAX is determined to be around 0.5 for spruce forests.

4) LOCATION: The Location file contains parameters specific to the geographical location determining radiation input, snowmelt, precipitation patterns (average daily duration of precipitation for each month DURATN) and vegetation patterns including parameters for seasonal changes in vegetation height and LAI throughout the year (RELHT and RELLAI as a fraction for specified doy). The RELLAI can be used to simulate phenology changes throughout the year and can account for both shedding of leaves from deciduous canopies and stomatal closure during winter.
5) FIXED & INITIAL: These two files include indices and set parameters needed for initiating the model run that were empirically determined and are typically not altered when fitting the model. They can be changed, but the set values should work for all environments robustly and it is difficult to estimate reasonable ranges (Federer et al., 2003).

3.2.4 Assumptions and Limitations

The model includes several limitations and assumptions as it is a simplified representation of the hydrological processes of a site (described also in more detail by Federer (2002); Federer (Revised - April 9, 2021); Federer et al. (2003)). Firstly, the model applies the “Big leaf concept” assuming a single homogeneous leaf canopy without considering vegetation layers. This also does not allow for non-green leaves which can intercept rain but do not transpire or changes in the albedo with varying solar elevation, snow age or canopy cover. Secondly, BROOK90 cannot account for changes in the vegetation over longer time spans such as growth in height and LAI or long-lasting damages from e.g. droughts. Thirdly, regarding the soil properties, it does not allow for soil frost, low vegetation cover such as mosses and the model for canopy and aerodynamic resistance by Shuttleworth and Wallace (1985) assumes a bare, uniformly distributed soil. Lastly, snow evaporation is, according to Federer (Revised - April 9, 2021), not handled well with an arbitrary correction of Shuttleworth and Gurney (1990).

3.3 Adjusted Parameters for Hyltemossa

To parameterize the model to the conditions in Hyltemossa and achieve a better model fit, the parameters listed below were adjusted (Table 1). The model was then run with input data from the ICOS measurements (Heliasz, Mölder, et al., 2024), and the outputs were tested against the measurement data from ICOS (Heliasz, Kljun, Biermann, Holst, Holst, Linderson, Mölder, et al., 2024) for the year of 2020. Here the variables evapotranspiration (ET) and soil water content (SWC) for all five layers were taken to minimize the difference between measurement and model

with 2020 data in a regression analysis. The best fit was assumed when both the R^2 value was high and the slope of the linear regression was close to 1.

Table 1: Parameters of BROOK90 changed to fit the measured evapotranspiration (ET) rate and volumetric soil water content (SWC) in five soil layers at Hyltemossa for the year 2020. The parameters are given in different parameter files (Flow, Soil, Canopy and Location) and are based on the physical properties of the model site.

File	Parameter (Abbreviation)	Set Value	Tested values
Flow	Infiltration Depth (IDEPTH) in mm	500	750, 730, 1000
	Bypass flow depth (QDEPTH) in mm	0	500, 730
	Impermeable fraction (IMPERV)	0.3	0, 0.02, 0.05, 0.3
	Infiltration distribution (INFEXP)	1	0, 0.5, 0.75
Soil	Layer Thickness (THICK) in mm	40; 35; 125; 450; 700	
	Field Capacity Ψ (PSIF) in kPa	-10; -8; -10; -12; -8.5	-5.5, -8.5, -10.0
	Field Capacity Θ (THETAF)	0.39; 0.4; 0.39; 0.4; 0.39	0.2, 0.32, 0.37, 0.4
	Brooks exponent (BEXP)	5.39; 6; 5.5; 3.5; 4	3, 3.5, 4, 5.5, 6, 7
	Hydraulic Conductivity (KF) in mm/d	6.3; 5; 7; 6.5; 5	1, 3, 5, 6.3, 7, 10
	Stone Content (STONEF)	0; 0; 0; 0; 0.5	0.1, 0.2, 0.3, 0.5
Canopy	Albedo (ALB)	0.09	
	Maximum height (MAXHT) in m	24.4	
	Maximum LAI (MAXLAI)	5	AVG up to 4.92
	Internal Conductivity (MXKPL) in mm/day,MPa	8	2, 3, 4, 5, 8,
	Internal plant resistance (FXYLEM)	0.5	0.1, 0.6, 0.9
	Max Leaf Conductance (GLMAX) in cm/s	0.53	0.2, 0.3, 0.4, 0.6
Location	Latitude (LAT) in °N	56.1°N	
	Average Daily Precipitation Duration per month (DURATION) in h/day	4,3,3,2,2,2,2,2,2,3,3,4	

Variation of LAI (RELLAI) (at day: 1, 54, 84, 299, 329, 366)	0, 0.5, 1, 1, 0.5, 0	1 (all year)

The MAXLAI, MAXHT and Albedo (ALB) are based on the measurements done by ICOS between 2018 and 2024 (Heliasz, Mölder, et al., 2024). Because of a lack of information on the soil properties, the soil layers and their thickness were set to fit the measurement depths of the ICOS sensors, at 30 mm, 50 mm, 100 mm, 300 mm, and 1000 mm depth, with a soil layer ending in the middle of two sensors. All parameters not specified here were taken from default parameter files provided by the model producer (Federer, 2019; Federer, Revised - April 9, 2021). The canopy file was for temperate evergreen forest (CTemperateEvergreenForest), the soil file for loam (SCl), the flow file for a top-down wetting front (FTopdown), the location file for Atlanta (LAmd) and the default Fixed and Initial files were used (Xdefault and Idefault). The location file was altered based on information on the site from Heliasz, Mölder, et al. (2024) and the average daily duration of precipitation per month was calculated from the meteorological data measured by ICOS between 2018 and 2024. The RELLAI is here loosely based on the vegetation period of Norway spruce and the seasonal pattern in the measured ET rate (Pastorello et al., 2020; Roloff et al., 2010), starting in February (doy 54) with reduced LAI by 50% and reaching the maximum LAI in March (day 84). The fraction value is then linearly interpolated between the set parameter values. This results in changes in both interception and transpiration rates throughout the year, with "RELLAI = 0" resulting in a LAI of 0.00001 and therefore strongly limited interception and transpiration. The other parameters were then adjusted one at a time and values were chosen when the best fit to the 2020 measurement data was achieved and all other parameters not shown in Table 1 are additionally displayed in Appendix 1. These parameters were used for all following modelling steps if not specified otherwise.

3.4 Data

Table 2 shows the data sets used as input for the BROOK90 model and to assess the model accuracy.

Table 2: Data used as model input for BROOK90 and for regression analysis of model outputs including the name of the data set and reference, variables used from the data and time coverage.

Data	Variable(s) (Unit)	Time Frame
ICOSETC_SE-Htm_ANCILLARY__20231023154450_INTERIM_L2 (Heliasz, Mölder, et al., 2024)	LAI (m^2/m^2), Canopy height (m)	2016 to 2023
ICOSETC_SE-Htm_METEO_INTERIM_L2 (Heliasz, Mölder, et al., 2024)	Precipitation (mm), Temperature (°C), Relative Humidity (%), Windspeed (m/s), Incoming Shortwave Radiation (SW_in, W/m^2); Soil water content (%) at 5 levels (30, 50, 100, 300, 1000 mm)	2018 to 2024

ICOSETC_SE-Htm_FLUXES_INTERIM_L2 (Heliasz, Kljun, Biermann, Holst, Holst, Linderson, Mölder, et al., 2024)	Latent Heat Flux (W/m²)	2018 to 2024
ICOSETC_SE-Htm_FLUXNET_HH_L2 (Heliasz, Kljun, Biermann, Holst, Holst, Linderson, Mölder, & Rinne, 2024)	Gap filled data: Precipitation (mm), Temperature (°C), Relative Humidity (%), Windspeed (m/s), Incoming Shortwave Radiation (SW_in, W/m²); Soil water content (%) at 5 levels (30, 50, 100, 300, 1000 mm), Latent Heat Flux (W/m²)	2018 to 2024
Station data from Helsingborg A (HelsingborgA, 2024a, 2024b, 2024c, 2024d)	Daily Minimum, Maximum, Average Temperature (°C); Hourly Wind Speed (m/s); Relative Humidity (%)	1995 to 2024
Station data from Klippan (Klippan, 2024)	Daily Precipitation (mm)	1945 to 2024
Station data from Ljungbyhed (LjungbyA, 2024; Ljungbyhed, 2024a, 2024b, 2024c)	Daily Minimum, Maximum, Average Temperature (°C); Hourly Wind Speed (m/s); Relative Humidity (%)	1950 to 2000
Global Radiation data from Lund Sol (LundSol, 2024)	Hourly Incoming Shortwave radiation (W/m²)	1983 to 2024

As the BROOK90 model requires daily precipitation, maximum and minimum temperature, these measurements were acquired from the ICOS station measurements (for April 2018 to December 2023) and the closest SMHI weather stations, which are in this case Klippan for precipitation data, Ljungbyhed and Helsingborg A for temperature, wind speed, and humidity data (Table 2). The ICOS measurements were done at different heights, with latent heat flux and wind speed at 27 m height, precipitation at 2 m at a different location, relative humidity and air temperature at 24 m and short-wave radiation at 50 m height. Since the model requires input and produces outputs in a daily resolution, the gap-filled data from ICOS was chosen here to minimize bias created by missing data in the daily averages (temperature, relative humidity, and wind speed data) and sums (precipitation, solar radiation, and latent heat flux). This was provided by Heliasz, Kljun, Biermann, Holst, Holst, Linderson, Mölder and Rinne (2024) and the data was gap-filled using the marginal distribution sampling (MDS) method, which approximates the atmospheric fluxes based on covariance with the meteorological drivers air temperature, incoming shortwave radiation and vapour pressure deficit as well as temporal autocorrelation (Pastorello et al., 2020). The incoming short-wave radiation, air temperature and wind speed data were additionally gap-filled with the ERA-interim method for values, where the MDS performance was unsatisfactory (Pastorello et al., 2020; Vuichard & Papale, 2015). Furthermore, the incoming shortwave radiation and latent heat flux data (LE) were corrected for a closed energy balance. For all variables, no

measurements were done between 01/01/2018 and 18/04/2018 meaning that input data as well as SWC and LE for this period is interpolated with the MDS or ERA-interim method and no SWC data is provided after 12/07/2022, because the sensors were damaged by a lightning strike (Heliasz, Mölder, et al., 2024).

The relative humidity (daily average in %) and average daily temperature was used to estimate the vapour pressure according to the Clausius–Clapeyron (C-C) relation approximation for saturation vapour pressure for horizontal liquid surfaces with temperatures above 0°C (empirical relationship) (Dingman, 2015):

Equation 2

$$RH = \frac{e}{e*} * 100\%$$

Where RH is the relative humidity in the air (%), e is the actual vapour pressure (in kPa) and e* is the saturation vapour pressure (kPa).

Equation 3

Station	T_{max}	T_{min}	Gap fill method
SMHI Ljungbyhed	04/12/1951 to 13/11/1952 09 – 10/10/1954;	23 – 26/03/1952 31/01/1952,	Filled in using T_{max} from Kolleberga or T_{min} if data was missing completely.
SMHI Helsingborg A	10 – 13/04/1998 04 – 10/01/1999 26 – 31/07/1999 17 – 20/09/1999		Set to 0 or T_{min} and output removed from after the model run.

$$e* = 0.611 \times exp^{\frac{17.3*T}{T+273.3}}$$

Where T is the air temperature (in °C).

The incoming shortwave radiation was measured at the closest location in Lund in the unit of W/m². Therefore, the data was transformed to be in MJ/(m², day) as specified by the model. All missing values in radiation, wind speed and vapour pressure were corrected to 0 as the model uses potential or default values and precipitation was also assumed 0 for any missing values. This was not possible for the temperature data as the model would stop working.

The temperature data was missing in the different datasets for the following periods:

Table 3: Periods of missing Input Data - Daily Maximum (T_{max}) and Minimum Temperature (T_{min}) from different Measurement Stations (Ljungbyhed and Helsingborg A) and method used to fill the data gaps.

Since Ljungbyhed is closest to the forest in Hyltemossa, its station data was used fully and filled up with adjusted data from Helsingborg A, Kolleberga and Klippan to achieve a full input time series. The temperature data was taken from Kolleberga for 01/01/1950 until 31/12/195, from Ljungbyhed from 01/01/1951 to 17/06/2001 and then Helsingborg A from 18/06/2001 until 30/11/2023. To account for temperature differences between Helsingborg and Hyltemossa the temperatures were adjusted according to the linear relationship between the datasets:

Equation 4

$$T_{MAX,Ljungbyhed} = \frac{T_{MAX,Helsingborg\ A}}{0.9595} - 0.469$$

$$T_{MIN,Ljungbyhed} = \frac{T_{MIN,Helsingborg\ A}}{0.8899} - 1.9621$$

The precipitation data was taken fully from Klippan as the station provides data for the entire period (01/01/1950 to 30/11/2023). Similarly, the global radiation data was taken from Lund Sol for 01/01/1983 until 30/11/2023 as there are no other stations measuring solar radiation closer to Hyltemossa.

The wind speed (WS in m/s) data was taken from Ljungbyhed between 01/01/1950 and 17/06/1995 and from Helsingborg A between 17/06/1995 and 30/11/2023. The data from Helsingborg was again adjusted according to the linear relationship to the data from Ljungbyhed for overlapping time periods:

Equation 5

$$WS_{Ljungbyhed} = \frac{WS_{HelsingborgA}}{0.9781}$$

The relative humidity data from 01/01/1950 to 01/01/1995 was taken as an average between Helsingborg and Ljungbyhed as both stations displayed large periods with missing data and then from Helsingborg A from 01/01/1995. Here, the average temperature to calculate the vapour pressure was taken from Ljungbyhed again until 1995 and from Helsingborg until 30/11/2023 and missing values were filled using the average of the measured maximum and minimum temperatures.

3.5 Model Application

As specified in the aim (Chapter 1.1), the model was first run with measured input data from the ICOS station (Heliasz, Mölder, et al., 2024). As the measurement intervals were 30 min, it was transformed to daily data by either summing (incoming radiation, precipitation), averaging (temperature, relative humidity, wind speed) or finding the extreme values (minimum and maximum temperature).

To perform the accuracy assessment, the measured and gap filled latent heat flux (LE) and soil water content data at the five different levels (30, 50, 100, 300 and 1000 mm) were then used to compare to the model outputs of ET and SWC for five layers, using the adjusted model parameters described in Chapter 3.3. First, the actual evapotranspiration rate (ET in mm/day) was approximated with LE (measured in W/m²), which is the energy transported with the water vapour flux. To convert the unit, the LE values were multiplied by the time interval in seconds (1800 seconds), divided by 1,000,000 (from J to MJ) and summed for each day to calculate the daily LE in MJ/m². The evaporation rate (ET in mm/day) is then given by:

Equation 6

$$LE = \delta_{Water} \lambda_{Vapour} ET \times 1000$$

where δ is the mass density of water in kg/m³, λ is the latent heat of vaporization in MJ/kg and 1000 is scaling factor for the density.

Equation 7

Where,

$$\lambda_{Vapour} = 2.50 - 0.00236 * T$$

With T being the air temperature in °C.

The model was validated using a linear regression analysis comparing the measurements and the model outputs. Higher accuracy was shown the higher the R^2 was and the closer the linear slope to 1 (Salciccioli et al., 2016). Here, dates with either missing measurement data or model inputs were not used as they would create a bias in the regression analysis. This is also the case for the data between 01/01 to 18/04/2018, where no measurements were done, but gap filled data is provided. Because it was utilized to parameterize the model to the site conditions and would therefore create a bias in the validation, the data from 2020 was not used. The same was done with model outputs based on the SMHI input data from the closest weather stations for 2018 to the end of 2023. Again, all periods with missing data were removed for the accuracy assessment given that they do not represent the model output. Moreover, the differences and linear regression between the model and measurements were tested for significance ($p < 0.05$).

To model the water balance of the forest since 1950 the BROOK90 model was then run with input from the weather stations as specified above.

3.5.1 Assumed Changes in LAI and Tree Height between 1950 and 2024

Since the forest does not remain constant in height (MAXHT) and leaf area index (MAXLAI) over a period of 80 years, these parameters were adjusted in five-year steps, as shown in Figure 2, according to the following assumptions:

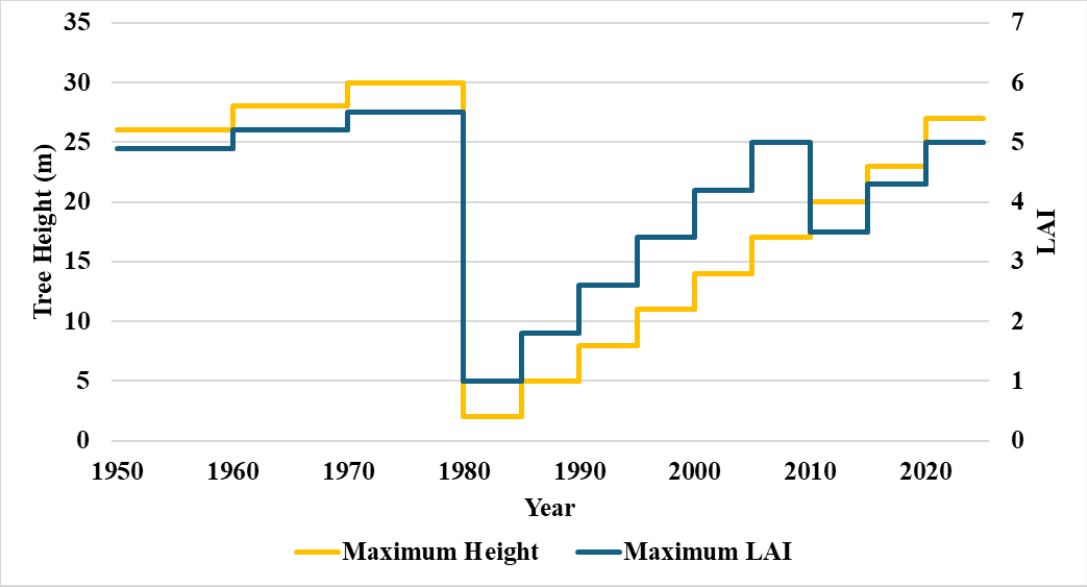

Figure 2: Assumed maximum LAI and maximum (tree) height at Hyltemossa for the BROOK90 model run from 1950 to 2025.

The maximum tree height (MAXHT) was adjusted according to the following assumptions. Literature suggests that trees show sigmoidal growth curves with Norway spruce exhibiting typically the highest growth rate at the age of 20 to 40 (Roloff et al., 2010; Weiner & Thomas, 2001; Zeide, 1993). This rate typically ranges from 0.01 m to 4.6 m in 5 years with an average increase of 1 m in five years (Huuskonen et al., 2023; Kindermann et al., 2018; Lee et al., 2024; Pretzsch et al., 2020). Here, however, the focus is on two different forest stands with different ages and properties which are lumped in BROOK90. This means that the MAXHT should represent both stands simultaneously. To represent both forests with adequate accuracy a linear growth in

the maximum tree height was assumed. The forest before the storm damage in 1982 and the clearcuts in 1983 and 1988 was assumed to be at the end of a turnover period (50 years old). Therefore, the maximum height was set to 30 m in 1980 with an increase of 4 m since 1950 (1m/5years). Due to the clearcut in 1983 and 1988, respectively, the MAXHT was assumed 0 for that year and 2 m for the 1980 to 1985 time step with a linear increase to the measured MAXHT 27 m between 2020 and 2025, resulting in a growth rate of 3 m/5 years (Heliasz, Mölder, et al., 2024). It was assumed to not be affected by cleaning or thinning since these practices typically remove small trees and non-spruce trees (Roberge et al., 2020).

Similarly, the maximum LAI (MAXLAI) was assumed to increase linearly with high values of 4.9 to 5.5 before the clear cut in 1980, and therefore slightly higher than the measured LAI by ICOS between 2016 and 2024 (Heliasz, Mölder, et al., 2024). Between 1980 and 2024 the change in LAI was assumed to be linear with a MAXLAI of 1.5 for 1980 to 1985, again taking into consideration the still full grown second stand before 1988. The increase was assumed to be 0.8/5 years and due to the thinning in 2009 and 2013 of the first stand and in 2015 of the second stand the LAI was reduced by 30 % from 5 to 3.5 for 2010 to 2015, reaching a final MAXLAI of 5 in 2020 to 2024. This rate is slightly smaller than observed by Pokorný et al. (2008), but a linear relationship between stand age and LAI is reportedly appropriate for young spruce forests.

3.5.2 Identification of Periods exhibiting Water Stress

Vegetation water stress can described by the fraction of actual transpiration over potential transpiration (Hammel & Kennel, 2001; Wellpott et al., 2005) also called the transpiration index (AT/PT). A transpiration index vluae below 1 typically indicates water stress (Federer, 2002). According to Hammel and Kennel (2001) a site experiences water deficiency frequently when the 25^{th} percentile is below 0.95. This value was used here to determine whether the site is frequently dry over the entire model period (1950 to 2024). Furthermore, years with an average transpiration index below 0.95 were identified as dry years and the number of dry days was calculated by counting all days within a year where AT/PT was smaller than 1, indicating water stress. Additionally, a regression analysis was performed, to test for significant trends ($p < 0.05$) in the transpiration index, ET rate, SWC as well as precipitation and temperature since 1950.

3.5.3 Scenarios

To compare the impact of different management strategies as well as the projected temperature increase with climate change on the water balance and experienced water stress, the following scenarios were applied by running BROOK90 with changed parameters or input data.

1. The **base line** scenario was based on stand properties measured and determined by ICOS and adjusted to achieve the best fit for the year 2020. This includes input parameters in the Flow, Canopy, Location and Soil files for the BROOK90 model (Chapter 3.3).
2. To model the impact on water stress of a higher stand density of the spruce forest, assuming no thinning was done during the growth of the forest, the leaf area index (LAI) was increased by 25%. This was applied by changing the leaf area index parameter MAXLAI from 5 to **6.25**.
3. To model the impact of a decreased stand density, assuming additional stand thinning, the MAXLAI was decreased by 25% from 5 to **3.75**.
4. To model the influence of rising temperatures due to **climate change**, the daily maximum and minimum temperatures were increased by 2 °C in the input data file. This value was chosen because according to Seneviratne (2023) and Lee et al. (2021) air temperatures will

increase in Scandinavia on average by 1.8°C to 4°C by 2100, depending on the forcing scenario (RPC 2.6 to RPC 8.5). Moreover, the relative humidity as well as the precipitation are assumed to be unchanged, because the changes show lower confidence and higher regional variability (Lee et al., 2021).

All scenarios were run with the gap filled weather data measured by ICOS at Hyltemossa from 2018 to 2024 (Heliasz, Kljun, Biermann, Holst, Holst, Linderson, Mölder, & Rinne, 2024). The difference between the scenarios regarding their ET rate, SWC, water stress and number of dry days were tested for significance ($p < 0.05$).

4 Results

4.1 Model Parameterization to 2020 ICOS data.

The model parameterization was adjusted using measured latent heat flux and volumetric soil water content data from ICOS (Heliasz, Kljun, Biermann, Holst, Holst, Linderson, Mölder, & Rinne, 2024). It resulted in a modelled evapotranspiration rate curve mostly following the pattern of the measured latent heat flux (Figure 3). As shown in Figure 3, the model produces mostly a higher ET rate than the measurements in the winter months (January to March and November to December, average difference of 0.31 mm/day) and a generally lower rate in the summer and early autumn months compared to the measurements (July to October, average difference of 0.35 mm/day). In contrast, spring and early summer (March to end of June) show smaller differences with the model being 0.16 mm/day higher on average than the measurements. The months showing the largest difference are July and August, where the model is lower than the measurements by about 0.62 and 0.6 mm/day on average, while it is higher by about 0.51 mm/day on average for February. The month where the modelled ET rate fit the measurements most is May with an average difference of 0.013 mm/day. Furthermore, the days with the largest discrepancies between modelled outputs and measurements are the 17/08 and 11/08 with a difference of 2.11 mm/day and 1.91 mm/day respectively (model is lower), as well as the 01/06 and 28/06 with 2.34 mm/day and 2.17 mm/day respectively (model is higher).

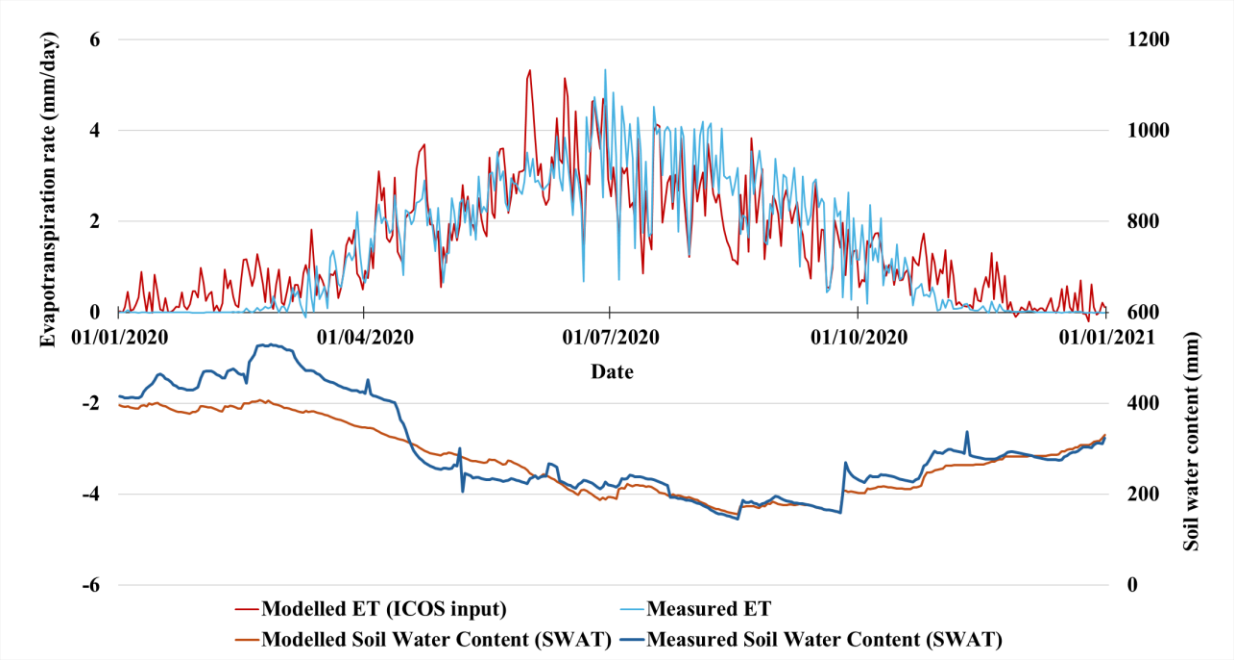

Figure 3: Modelled and Measured daily evapotranspiration (ET, in mm/day) and soil water content throughout entire soil column (SWAT, in mm) at Hyltemossa for 2020 after parameterizing BROOK90 with latent heat flux (LE) and volumetric soil water content data from 2020.

The results of the regression analysis are shown in Table 4 and Figure 4, displaying that the modelled ET rate is on average higher than measured (by about 2%), however with the model generally underestimating it with a linear regression slope of 0.9. The modelled ET rate shows a

high fit to the linear regression model with an R^2 of 0.89 and this is also reflected in the similar value ranges and low average difference, which is not significant ($p > 0.05$).

Table 4: Statistics on the BROOK90 model after parameterization with 2020 data comparing modelled evapotranspiration rate (ET) and volumetric soil water content (SWC) for all five soil layers (1 to 5) to the measured measurement data by ICOS. The statistical variables include slope of the linear regression, the R^2, average difference (measured – modelled value), standard deviation (STDV) of the difference between model and measurement and the range of the model outputs and measurements.

Statistical Variable	ET (mm/day)	SWC 1	SWC 2	SWC 3	SWC 4	SWC 5
Regression Slope	0.90	1.12	1.18	1.13	1.17	1.41
R^2	0.89	0.99	0.99	0.99	0.99	0.82
Average Difference	-0.04	-0.01	-0.01	0.005	-0.001	0.11
STDV of Difference	0.68	0.03	0.03	0.03	0.05	0.05
Range Model	-0.2 to 5.33	0.15 to 0.37	0.16 to 0.37	0.15 to 0.38	0.11 to 0.42	0.20 to 0.41
Range Measured	-0.11 to 5.34	0.14 to 0.39	0.12 to 0.37	0.15 to 0.41	0.16 to 0.41	0.06 to 0.42

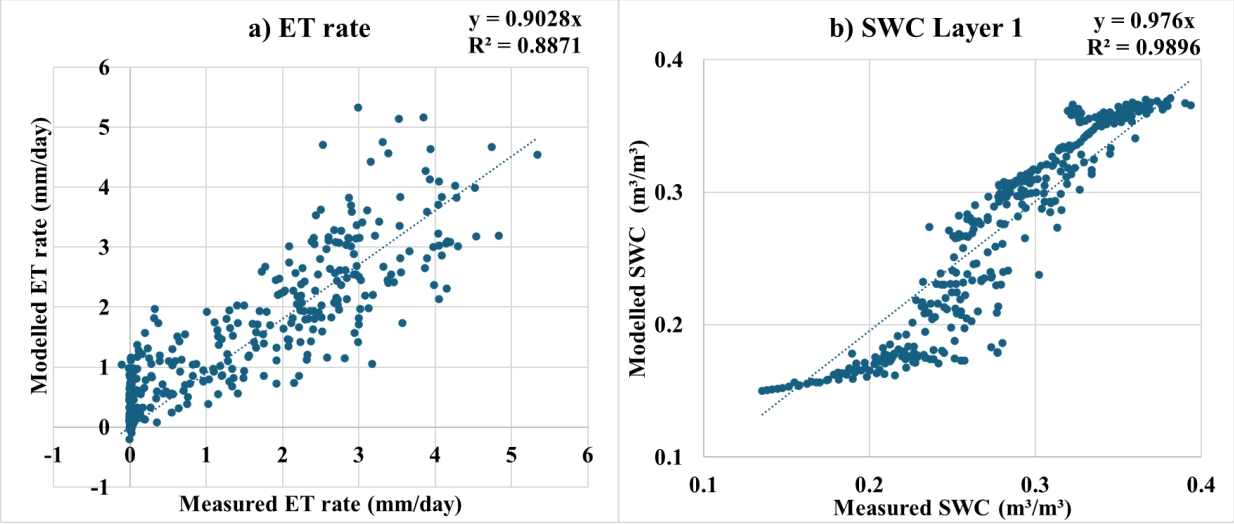

Figure 4: Regression analysis of the model outputs after parameterizing BROOK90 with the measured data from 2020. The modelled daily a) evapotranspiration (ET) and b) volumetric soil water content (SWC) are compared to measured data from Hyltemossa in a scatter plot, showing the slope and R^2 of the linear regression.

The soil water content for all layers is generally higher in the model, with the linear slope ranging from 1.12 to 1.41, with the first four soil layers showing a very high fit (R^2 of 0.99) and the model outputs for layer five a slightly worse fit (see also Appendix 2 and 3). The ranges of SWC are similar between the model and measurements and the model outputs for all layers and

show generally a low average difference to the measurements (ranging from 0.001 to 0.11), with slightly higher values for the fifth layer.

Similarly to the ET rate the annual pattern of high soil water content in winter and low values in summer as measured at Hyltemossa are reflected well by the model outputs (Appendix 2). The model output shows generally higher short time variations than the measurements, which are greatest in summer (June to September) for all layers. Except for Layer 5, the model values are higher than the measurements in winter and spring (January to May and November and December) and lower during summer and autumn (May to November). The soil layer showing the greatest deviations between the modelled and measured water content is the fifth layer at approximately 1 m depth. This is especially evident from April and onwards.

4.2 Input Data – Comparison of ICOS and SMHI measurements.

According to the data from 1950 to 2023 from the different SMHI stations, the site has an annual precipitation of on average 756.4 mm ranging from 462.2 mm in 2018 to 1077.8 in 1998. The site shows an average temperature of 7.72 °C with the maximum temperature ranging from -6.8°C to 29.8°C and the minimum temperature from -17.4 to 17.4°C and an average daily temperature range of 8.1°C (Figure 5). One can observe a significant positive trend in temperature since 1950 with a difference of 1.1°C between 1950 to 1980 and 1981 to 2024. In contrast, precipitation shows no significant trend throughout the measurement period. Furthermore, the data displays an average windspeed of 3.57 m/s, average vapour pressure of 0.79 kPa and daily net radiation of 5.56 MJ/m².

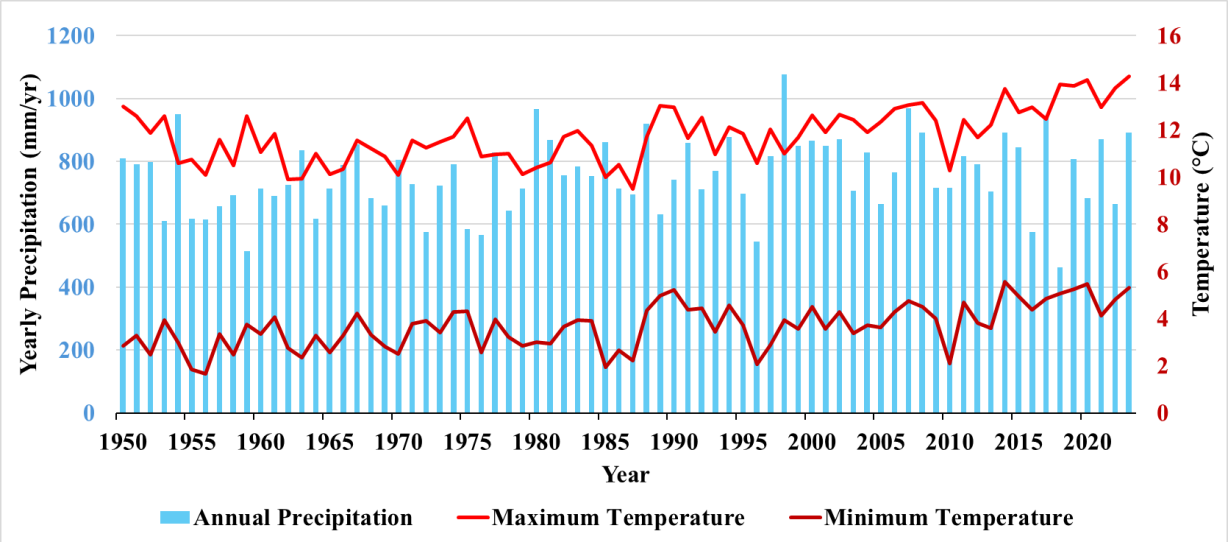

Figure 5: Annual total precipitation and average maximum and minimum temperatures at Hyltemossa based on measurement data from nearby SMHI stations for 1950 to 2023.

To assess the differences between the measured input data, measurements from the closest SMHI station and from ICOS at Hyltemossa were plotted in scatter plots (Figure 6).

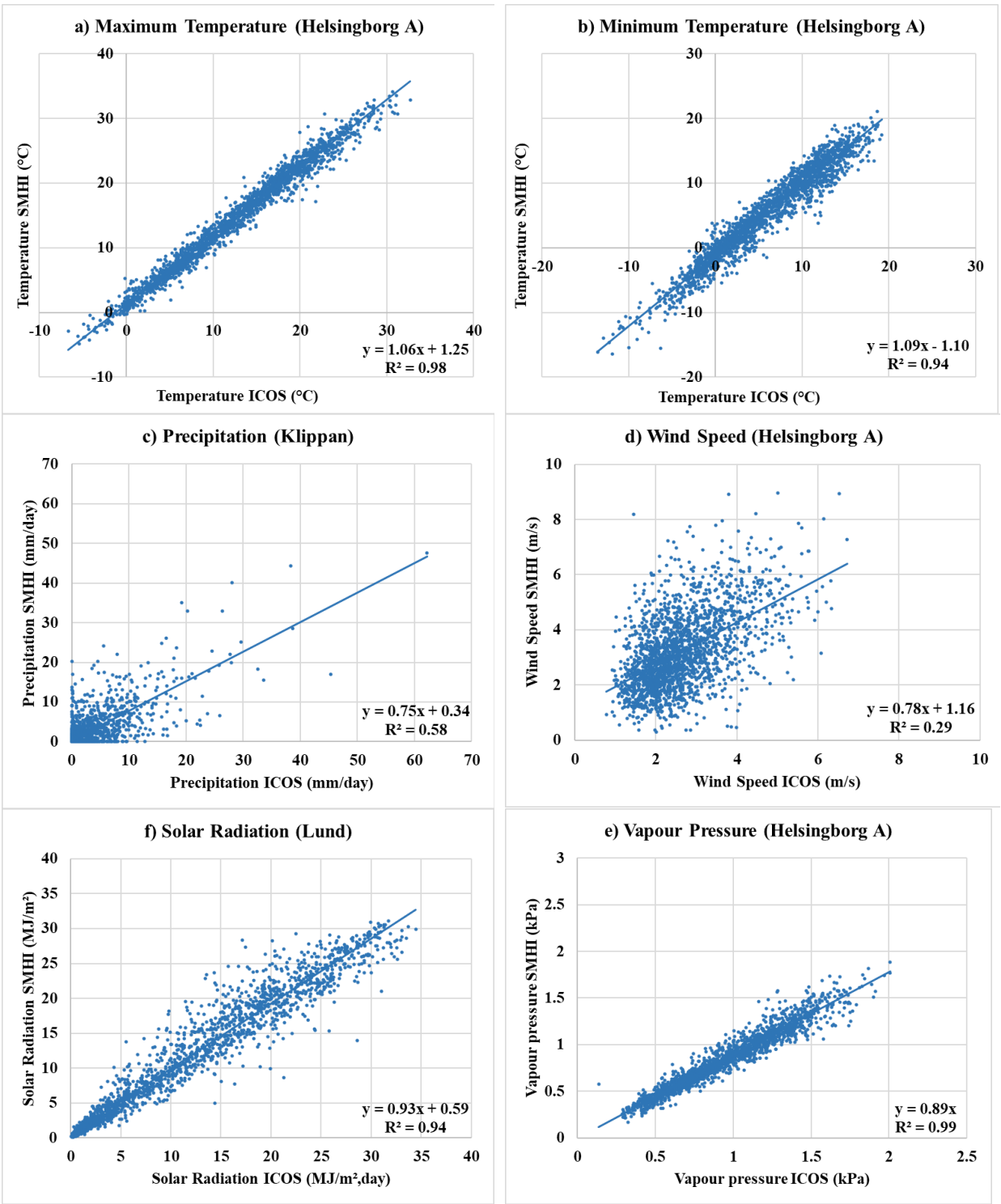

Figure 6: Comparison of measured input data from ICOS at Hyltemossa and nearby SMHI meteorological stations (name in brackets) in linear regression analysis including linear equation and R². The input variables are daily a) Maximum Temperature, b) Minimum Temperature, c) Total Precipitation, d) Average Windspeed, e) Average Vapour pressure and e) Total Incoming Solar Radiation for 2018 to 2023.

Comparing the data sets, one can see that temperature and wind speed are both generally higher at the SMHI station in Helsingborg A than in Hyltemossa (Figure 6). In contrast, the measured vapour pressure in Helsingborg A and solar radiation from Lund Sol are overall lower than measured by ICOS, with both showing a nearly linear relationship (high R^2 and slope close to 1). The measured precipitation shows, together with wind speed, the highest variation between the datasets (R^2 of 0.58 and 0.29), with higher precipitation typically occurring at Hyltemossa compared to the SMHI station in Klippan (Figure 6). There are no obvious seasonal patterns regarding the differences between the datasets and except for the precipitation data, the input data sets vary in similar yearly and seasonal patterns.

4.3 Model Validation for 2018 to 2024.

When comparing the ICOS measurements and modelled ET rate for the full data range (January 2018 to December 2023), one can see that both follow the same seasonal pattern with low to no evapotranspiration in late autumn and winter (November to March) and the highest rates in summer (May to June), as shown in Figure 7. The outputs have an average yearly range of -0.2 mm/day to 5 mm/day in the measured data and -0.7 mm/day to 6.2 mm/day in the model outputs.

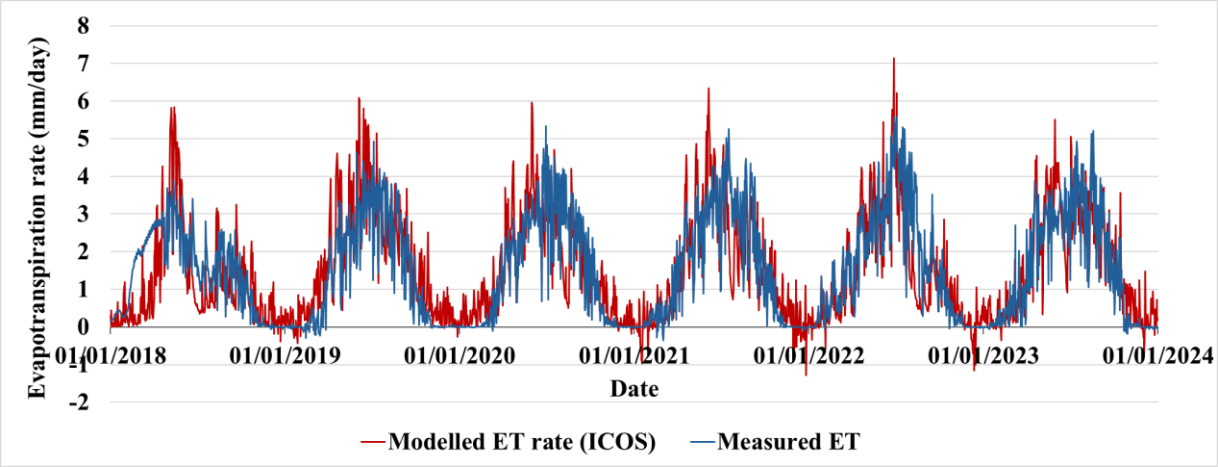

Figure 7: Comparison of gap-filled measured (blue) and modelled (red) evapotranspiration rate (ET) based on ICOS input data for 2018 to 2023 at Hyltemossa.

As shown in Figure 7, the model outputs show on average higher ET rates in autumn and winter (October to March) by about 12% and late spring (May and June) by about 22%, which is most prominent in 2019. In contrast, the ET rates measured by ICOS for summer and early autumn (July to October) are generally higher than the modelled ones on average by 31 %. It should be noted that the measured and input data for January to the 19th of April 2018 is purely gap filled data, since no actual measurements were made during that period, which is reflected in the smooth curve of measured ET rates.

As shown in Table 5, the modelled ET rates show a greater value range than the measurements, with the model outputs based on SMHI input data (SMHI model) showing the highest range. Furthermore, the ET (SMHI) displays higher average difference and range of differences to the measurements compared to ET (ICOS), with both showing higher ET rates than measured on average by approx. 5% and 1%, respectively. This difference is no significant for the ICOS model outputs but significant for the SMHI model outputs. In contrast, the linear slope is always smaller

than 1 meaning that the linear regression shows an underestimation of the measured ET rate (Figure 8, Table 5). Here, the slope is smaller for ET (SMHI) than for ET (ICOS) with a greater spread from the linear relationship (smaller R^2 at 0.74 compared to 0.84). This goes also for the soil water content, which shows for both model outputs closer fits to the measurements than the ET rate. The soil water content is overall lower in the model outputs than the measured data with the ICOS inputs showing again a better fit and a smaller difference of on average 5% less than the measurements compared to 12% for the SMHI SWC.

The other four soil layers show similar properties, with the modelled SWC showing higher values than the measurements by about 10 to 15 % (SMHI input) and 3% (ICOS input) for layers 3 and 4 and higher values by on average around 2% (SMHI input) and 8% (ICOS input) for layer 2. Layer 5 at a depth of 1 m shows the biggest differences between the model outputs and the measurements, with the modelled SWC showing on average approximately 30% (SMHI input) to 37 % (ICOS input) higher values than measured (see also Appendix 4).

Table 5: Properties of BROOK90 modelled ET rate and SWC in the first soil layer (SWC 1) for 2018 to 2024 using ICOS and SMHI measurements as input. This includes the data range, the average (AVG) difference between the model outputs ad ICOS measurements, range of the difference as well as the linear slope and R^2 of the linear regression of model and measurements.

Variable (Source)	Range	AVG Difference to Measurement	Range Differences	Linear Slope	R^2
Measured ET in mm/day	-0.36 – 5.59	0	0	1	1
ET (ICOS) in mm/day	-1.28 – 7.14	-0.015	-3.12 – 3.61	0.94	0.84
ET (SMHI) in mm/day	-2.12 – 2.76	-0.069	-4.86 – 4.26	0.87	0.74
Measured SWC 1	0.11 – 0.43	0	0	1	1
SWC 1 (ICOS)	0.15 – 0.39	0.01	-0.35 – 0.15	0.96	0.98
SWC 1 (SMHI)	0.15 – 0.38	0.03	-0.34 – 0.19	0.89	0.97

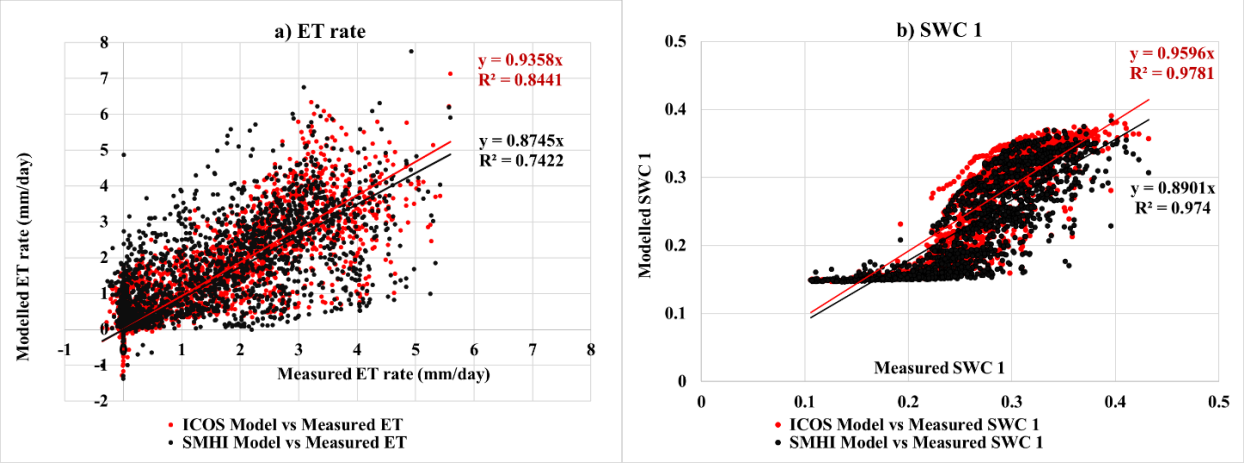

Figure 8: Linear Regression Analysis of Modelled vs Measured evapotranspiration rate (ET) and volumetric soil water content (SWC) in the first soil layer (1) comparing different input data sets (ICOS in red and measurements from SMHI stations in black). For the linear regression, the linear slope and R^2 are displayed.

When comparing the model performance for different years, one can see that the model produced outputs close to the measurements for 2018, 2020 and the beginning of 2021, 2022 and 2023 (Figure 9). The largest differences can be seen in 2019 where the model outputs are higher starting in January, show similar increase rates in spring and summer (April to October) and are increasing more than measured in autumn and winter (October to December), generally producing higher accumulative yearly ET than measured by 111 mm (SMHI) and 137 mm (ICOS). Similarly, at the end of 2018, 2021 and 2023 the model outputs are higher than the measurements at the end of the year starting in October, with total yearly differences of 39 mm, 73 mm, and 93 mm (SMHI) and 6 mm, 1mm and 32 mm (ICOS). The only year where the model outputs are lower than the accumulated measured ET is 2022, with differences of 64 mm (SMHI) and 68 mm (ICOS), which is also the year with the highest measured accumulated ET of 598 mm/year. Furthermore, the model using SMHI input data produces the higher yearly ET values than when using ICOS input data for most years (2018, 2021, 2022, 2023) with differences between the model outputs ranging from 4 mm/year in 2022 to 72 mm/year in 2021.

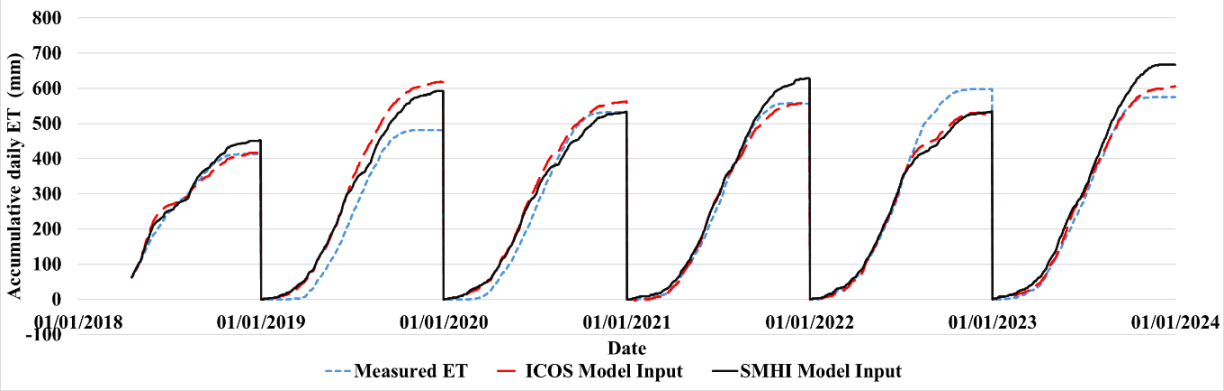

Figure 9: Daily Accumulated evapotranspiration rate (ET) comparing the measurements (Blue) and model outputs using different input data sets (from ICOS in red and SMHI stations in black) for 2018 to 2023 at Hyltemossa.

As shown in Figure 10, the ICOS input data shows lower water stress levels (higher Transpiration Index) than the SMHI data for all years except 2021, with an average transpiration index of 0.91 and 0.88 respectively.

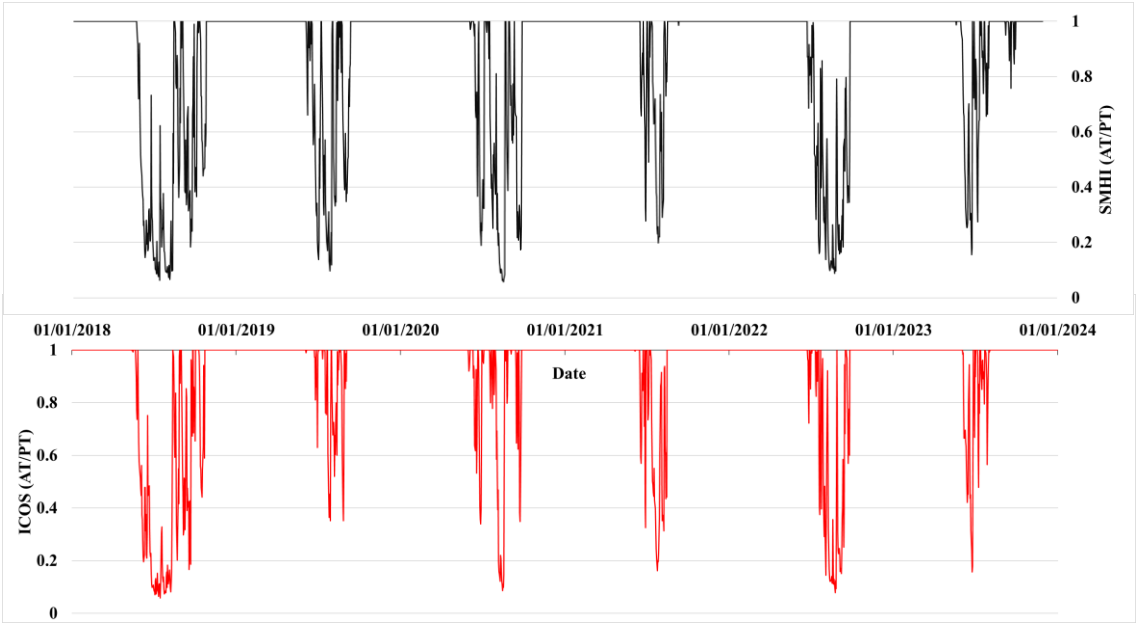

Figure 10: Comparison of modelled water stress given by the Transpiration index, AT/PT) using input data from nearby SMHI stations (top in black) and ICOS at Hyltemossa (bottom in red) respectively for the time frame 2018 to 2024 at Hyltemossa.

Both follow the same seasonal pattern with water stress typically occurring in Summer (between June and September or October) and almost no stress for the rest of the year (October to May). For some years, this period is slightly longer (2018 and 2020) or shorter (2021) with 2018 displaying the longest and strongest water stress period from the end of May until the end of October and an average transpiration index of approx.0.77 (for both models). In contrast, the years experiencing the least water stress, looking at the model with ICOS data are 2019 and 2023 with around an average of 0.96 and 2021 and 2023 with 0.94 when looking at the model with SMHI data. The years with the largest differences in water stress between the two model runs are 2019

and 2022 with the model using SMHI input data showing a lower average transpiration index value by 0.07 and 0.04, respectively. In contrast, the year 2018 shows the smallest difference between the model outputs with around 0.004.

4.4 Water Balance at Hyltemossa since 1950

The BROOK90 model was then run for the full SMHI input data from 1950 to the end of 2023, producing daily ET, PT and AT rates as well as water stress level based on the transpiration index (Appendix 5). As shown in Figure 9, the ET rate ranges for the entire period between -3.7 mm/day and 7.76 mm/day with an average of 1.4 mm/day, while the AT shows a range of 0 to 5.47 mm/day with an average of 1.01 mm/day (around 72% of the average evapotranspiration and 88% of the potential transpiration rate). Furthermore, both ET and AT are considerably lower from 1980 onwards based on the lower LAI following the replanting of the forest and reach rates like 1950 to 1980 by 2005 (Appendix 5).

As shown in Figure 11, the year with the lowest average and accumulated ET is 1984 with 0.67 mm/day and a total of 246.36 mm/year while the years showing the highest ET rate are 2007 and 2023 with an average of 1.8 and 2.0 mm/day and a total of 657.61 mm/year and 667.07 mm/year respectively. Furthermore, about 72 % of the ET rate is transpiration leaving around 28% or 0.39 mm/day on average for evaporation. The actual transpiration rate is typically close or the same as the potential transpiration rate especially between 1980 and 2002 with the largest differences in 1952, 2018 and 2022 showing an accumulative difference of 192 mm/year, 275 mm/year and 183 mm/year, respectively. For some years, the PT even surpasses the ET rate including 1951, 1952, 1959, 1976, 2018, 2020 and 2022 with 2018 showing a PT rate which is higher than the ET by 172 mm/year.

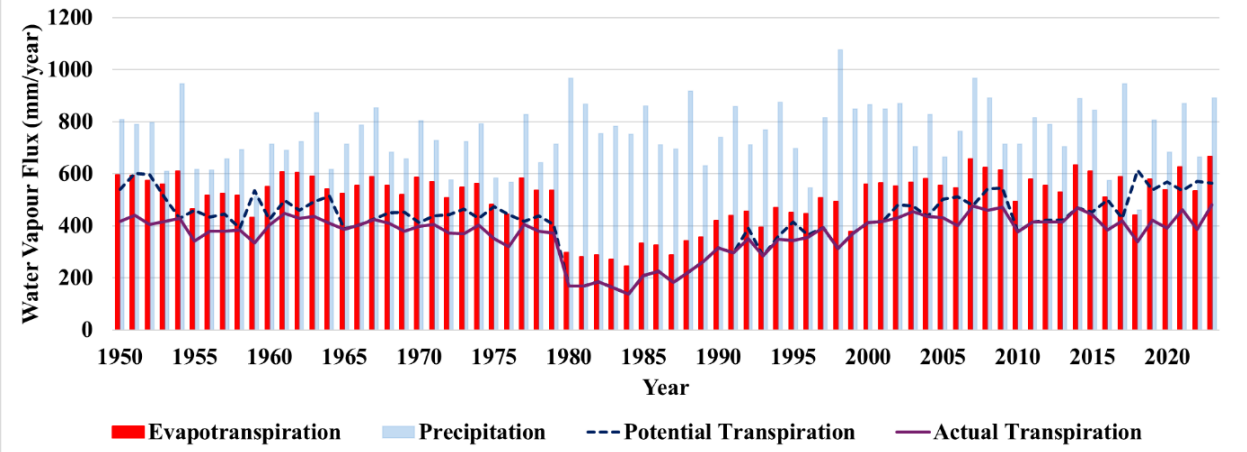

Figure 11: Modelled total annual evapotranspiration, potential transpiration, actual transpiration and measured precipitation at Hyltemossa for 1950 to 2023 using SMHI input data and assuming a changing leaf are index and tree height over time (Chapter 3.5.1).

When comparing the ET to the yearly precipitation, one can see that about 69% of the precipitation evaporates, leaving the rest of the water for storage and flow (overland or underground). This ration fluctuates between the years, with ET taking up about 78% of the precipitation before 1980, about 50% between 1980 and 2000 and around 74% after 2000. The largest difference between ET and precipitation can be found in 1980 where about 31% of the precipitation was ET, while 1953 and 2018 show the smallest difference with 92% and a little over

95 %, respectively. Here, the potential transpiration only surpasses the precipitation on two years which are 1995 and 2018 by 21.8 mm (4%) and 152.4 mm (33%), with an average of 57.6% of the precipitation being allocated for potential transpiration.

Looking at the modelled water stress for the period of 1950 to 2023, displayed in Figure 12, one can see that the transpiration index fluctuates between the years. It shows a similar pattern as the ET rate with low to no stress between 1980 and 2002 (high transpiration index) averaging at 0.99. Higher stress levels can be observed before 1980 and after 2002 with an average of 0.93 and 0.95, respectively. Overall, the site shows an average transpiration index of 0.96 with a standard deviation of 0.16 and values ranging from 0.06 (August 2020) to 1. It experiences water stress for on average 40 days a year, with the duration ranging between 0 (in 1966, 1980 to 1991, 1994, 1997, 2001, 2004 and 2011) and 135 days a year (in 2018). Furthermore, the 25th percentile is at 1, categorizing the site as not frequently dry.

Looking at the seasonal patterns, winter months (November to May) show typically low or no water stress while the summer months (July to October) show the lowest average transpiration index ranging from 0.83 in July to 0.87 in August, with intermediate values in spring and October of around 0.95.

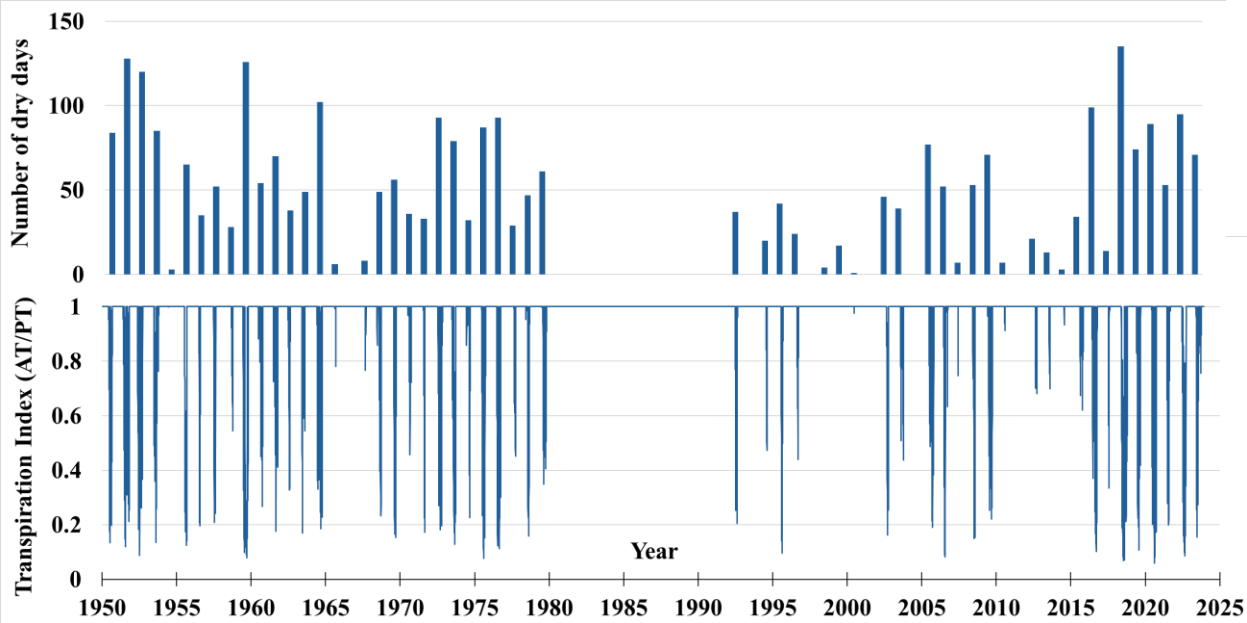

Figure 12: Modelled Water stress (bottom) and annual number of dry days (top) using the BROOK90 model and SMHI input data for the Forest in Hyltemossa between 1950 and 2024 represented by the transpiration index (AT/PT). A transpiration index of 1 indicates no stress.

The model showed the lowest average transpiration index for the years 1959 and 2018 with values of 0.789 and 0.792 respectively and a total of 126 and 135 days with an index value below 1. Furthermore, 11 more years showed an average value below 0.9 including 1950, 1951, 1952, 1955, 1964, 1972, 1975, 1976, 2016, 2020 and 2022, with 1951 showing the lowest value of those years with 0.843. For these, the number of days with water stress ranged between 65 in 1976 and 128 in 1951. Furthermore, it can be noted that none of the years of 1980 to 1991 would experience water stress with indices averaging below 0.9 if the forest was not cut down (assuming an MAXLAI of 5 and a MAXHT of 27 m). However, when assuming an unchanging forest LAI and height, the average stress would increase, resulting in an index of 0.95 (0.01 lower)(Appendix 6).

Furthermore, with a constant LAI there is a significant increase in ET of 0.85 mm/year and no significant trend in the soil water content, precipitation, the transpiration index, or the number of dry days per year ($p < 0.05$).

4.5 Scenarios

When comparing the outputs of the four scenarios assuming changes in the forest management (Scenario 2 and 3) or in the temperature assuming an increase by 2°C due to climate change, one can see that on average, the ET rate is the highest for Scenario 4 (CC), followed by Scenario 2 (LAI 6.25), the base line Scenario 1 and lastly Scenario 3 (LAI 3.75) (Table 6). Here, increasing the maximum LAI by 25% (Scenario 2) results in a significant increase of ET rate by on average 4 %, while a decreased LAI by 25% lowers the ET rate by 5% on average. This comes with a significantly increased water stress level (lower transpiration index) by 2 % for Scenario 2 and a decreased stress level by 3% for Scenario 3. Similarly, the soil water content is lowered on average by 6 mm (2%) and increased by almost 10 mm (4%) for the respective scenarios. Therefore, even though the change in LAI is by the same fraction, the decrease in LAI leads to a larger change in the model outputs than the increase. Looking at the climate change Scenario (4) one can see that the increase in temperature results in a significantly increased ET and AT rate (by 10% and 8%) with decreased soil water content (7%) and transpiration index (by 6%). Scenario 3 shows the largest range of values while the Scenario 4 shows the smallest. All differences between the scenarios mentioned above were tested for significance and show $p < 0.05$ and are therefore significant.

Table 6: Properties of output data from the four different scenarios (1 to 4) described in Chapter 3.5.3 including the average (AVG), standard deviation (STDV) and range of the evapotranspiration (ET) rate (mm/day), the average difference to the baseline scenario (1) as well as the average daily transpiration index (Stress), soil water content (SWAT in mm) and transpiration rate (AT in mm/day).

Scenario	**Measured**	**1 (Baseline)**	**2 (LAI 6.25)**	**3 (LAI 3.75)**	**4 (CC)**
AVG ET (mm/day) (STDV)	1.49 (1.39)	1.50 (1.38)	1.56 (1.41)	1.43 (1.34)	1.66 (1.36)
Range of ET (mm/day)	-0.36 – 5.59	-1.28 - 7.14	-1.3 – 6.7	-1.95 – 7.85	-0.07 - 6.37
AVG difference to ET baseline	0.02	-	-0.06	0.08	-0.15
AVG Stress (STDV)	-	0.91 (0.22)	0.89 (0.25)	0.94 (0.18)	0.86 (0.28)
AVG SWAT (mm) (STDV)	-	264.9 (80.5)	258.5 (80.8)	274.6 (78.7)	246.8 (79.5)
AVG AT (mm/day) (STDV)	-	1.13 (1.32)	1.13 (1.33)	1.10 (1.29)	1.21 (1.29)

When looking at the seasonal patterns and inter annual differences (Figure 13), it becomes apparent that Scenario 3 and 4 model water stress periods to start earlier (typically by one or two

days) to be more severe (up to 30 % lower transpiration index values) with the temperature increase showing more severe water stress values than higher stand density (Scenario 2). In contrast, lowered stand density is modelled to reduce both the duration of water stress periods and the severity (up to over 100% increase of the transpiration index from the baseline scenario) and sometimes showing no stress for periods where the other scenarios predict them (e.g., 09/07/2019 to 23/07/2019). The number of dry days (AT/PT < 1) is significantly increased for Scenarios 2 and 4 by on average 10.8 days and 29 days annually respectively, while the dry period is shortened on average by 23.5 days in Scenario 3 compared to the baseline of 73.3 days annually.

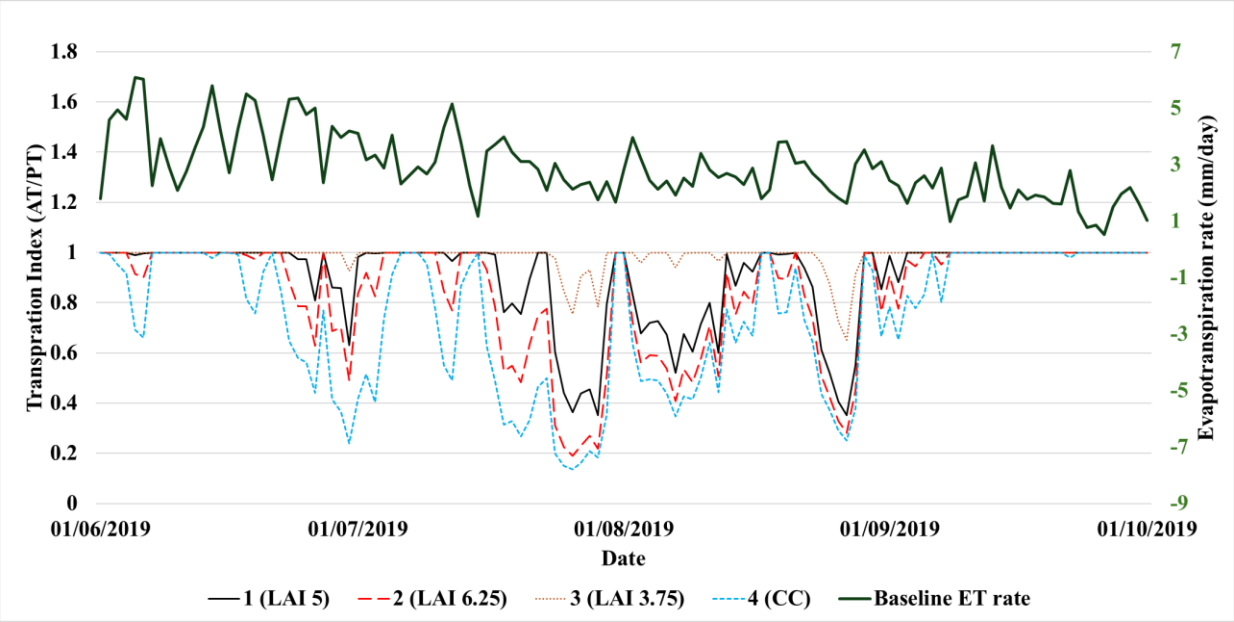

Figure 13: Comparison of modelled transpiration index for the four scenarios (1 – baseline, 2 – increased LAI, 3 – decreased LAI, 4 – climate change (temperature increase)) for the growing season of 2019. The evapotranspiration rate of the baseline scenario (1) is given at the top.

These seasonal patterns also depend on the different years and level of stress as shown in Figure 14. Here, 2018 is the year that displays the highest stress level (average transpiration index ranging between 0.73 and 0.81 depending on the scenario) and shows the smallest differences between the scenarios regarding its evapotranspiration rate (around 3 to 5% difference to the baseline). Similarly, the transpiration index shows a lower stress level in 2019 (around 0.91 to 0.99) with larger differences in the ET rates (4% to 12% difference from the baseline, see Figure 13 and 14).

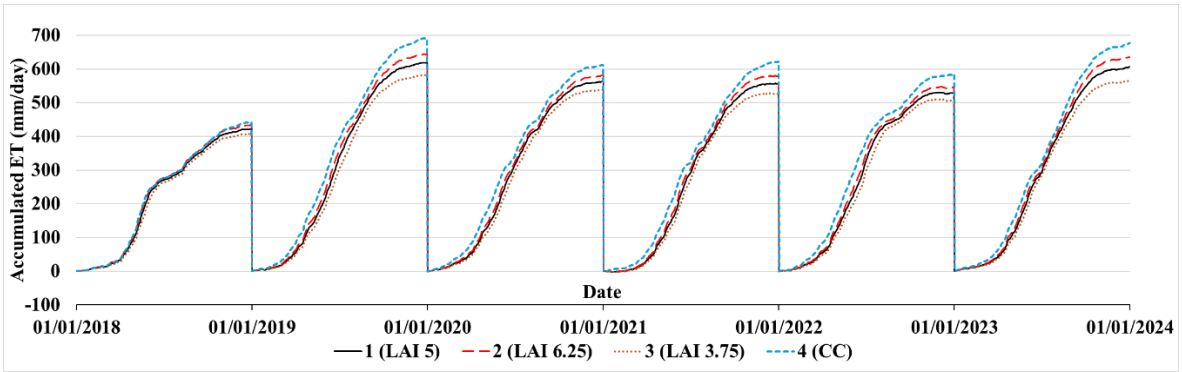

Figure 14: Comparison of the accumulative evapotranspiration (ET) rate for the four Scenarios (1 – baseline, 2 – increased LAI, 3 – decreased LAI, 4 – climate change (temperature increase)) between 2018 and 2024.

5 Discussion

5.1 BROOK90 Model validation for 2018 to 2024

Looking at the model validation, one can see that BROOK90 provides a good approximation of the site evapotranspiration rate and soil moisture content with the R^2 ranging from 0.74 to 0.98, reflecting the seasonal pattern and interannual trends relatively well. The model fit for 2018 to 2023 is slightly worse than for 2020 (showing an R^2 of 0.88 to 0.99), because the model was parameterized to fit the measurements from 2020. Compared to other studies using BROOK90, the model validation shows a good fit. For example, Luong et al. (2022), Tahir (2012) and Kronenberg et al. (2013) produced an ET model fit with an R^2 of 0.62, 0.26 and 0.95 respectively for pine forests or mixed forests. While Tahir (2012) generally overestimated the ET rate, Luong et al. (2022) produced overall lower results than the measurements. However, considering that site conditions and parameters differ between these studies, it is difficult to compare them and a specific parameter determining the differences in accuracy cannot be pinpointed. This is also displayed by Wellpott et al. (2005) and Tahir (2012), which both applied BROOK90 to the pine forest in Hartheim, Germany. While both studies found a robust model output, the study by Wellpott et al. (2005) showed a fit of 0.97 to the soil conditions, while Tahir (2012) study displayed a considerably worse fit with an R^2 of 0.55. This is most likely connected to the parameterization. Similarly, Vorobevskii et al. (2022) compares a tuned BROOK90 to a model run with arbitrary parameters, showing that especially the canopy and soil parameters determine the accuracy of the model outputs and uncertainty connected to the model.

In this thesis, all parameters chosen for the soil and flow properties were arbitrary since no data was provided on the water retention properties, soil profile or structure. Even though the model showed a very high fit to the measured SWC at the site, the actual soil might differ greatly from the chosen parameters. Therefore, determining the soil properties on site for the parameterization might improve the model, given that it is designed to utilize physically meaningful parameters. Nevertheless, this shows that the application of BROOK90 in areas where measurements are not possible or very costly can still produce robust results. The same goes for the root properties of the forest, which were not adjusted due to a lack of data. According to Federer et al. (2003) the model is however less sensitive to the root properties with the climate and weather conditions, canopy properties and soil structures showing the highest influence. Moreover, the latent heat flux measured at the site might not correspond fully to the soil water conditions.

Accordingly, the model input data and its accuracy are imperative. As shown in the results, the model performance was significantly better with input data from Hyltemossa compared to measurements from the closest SMHI station. With SMHI input, the model tends to overestimate the ET rate by approximately 5% and therefore also the experienced stress. This could be due to the differences in temperature and precipitation between the measurement sites (Figure 6). The temperatures measured at Helsingborg A are higher than at Hyltemossa, which is probably due to the measurement height. While the SMHI measures temperatures at the height of 2 m, the ICOS measurements were done at 24 m above the canopy, leading to lower values. This in turn results in higher ET rates with SMHI data. Similarly, the windspeed is higher in the SMHI inputs with lower vapour pressure which both generally produce higher ET rates. However, the most influential input is the precipitation, which differs the most between Hyltemossa and the SMHI station in Klippan. This most likely contributed most to the significant discrepancy between the measurements and model output on the daily resolution. Furthermore, because the input is in daily

resolution, it does not allow for detailed diurnal patterns. Therefore, evaporation could be allocated to the wrong day, which could explain some of the major differences between model and measurement on a daily scale. To improve on this, precipitation can also be provided in smaller time steps in the model, however, the historical data is rarely in higher temporal resolution, and it was therefore opted for daily input data.

Looking at the seasonal pattern, the model overestimates the ET rate in winter by 12 to 22 % depending on the input data. During this time ET is supposed to be nearly 0 mm/day due to low temperatures resulting in limited evaporation, possible soil frost and stomatal closure and therefore reduced transpiration. This overestimation was also found by most other studies using BROOK90 (Kronenberg et al., 2013; Luong et al., 2020; Vorobevskii et al., 2022). It can be most likely be attributed to the poor handling of snow evaporation and the assumption that soil does not freeze in the model, which is also discussed by Kronenberg et al. (2013). Here, frozen ground would limit the soil infiltration and evaporation, even though it rarely occurs at Hyltemossa due to the dense canopy cover. Furthermore, the model produces negative ET rates modelling condensation rates down to -2.12 mm/day, which was pointed out by Kronenberg et al. (2013) as highly implausible. They, thus, applied a correction, which should be considered in future applications of BROOK90. Given that the focus of this thesis is on water stress, which typically occurs in the summer months, the winter months were generally disregarded. For the growing season, the model performs overall better and underestimates the ET rate by up to 10%. Nevertheless, it overestimates the ET rate for early summer periods by up to 18% and underestimates it for later months by as much as 31%. This could be due to the applied seasonal LAI (RELLAI) pattern which defines an LAI ration of 0.5 at the end of February and 1 at the end of March, assuming a linear relationship between the two. However, spruce forests typically start the growing period in April, with temperatures rising rather late in southern Sweden which could explain the overestimation in spring and early summer (Przybylski, 2007; Roloff et al., 2010). Therefore, when evaluating the water stress coefficient, it should be expected that the model overestimates the length of the dry period as well as the stress in early summer and underestimates it in August and September, especially with the SMHI data.

The model validation comes with multiple limitations connected to the model and the data. First, as mentioned in Chapter 3.2.4, the model assumes a single layer, homogeneous, green canopy cover, disregarding understory vegetation and its contribution to the ET rate and SWC. It can contribute up to 50% to the transpiration rate depending on the LAI and sunlight extinction in the canopy (Luong et al., 2022). At Hyltemossa the ground is mostly covered by mosses, probably not contributing significantly to the transpiration rate. But it can lower the soil temperature and delay infiltration (Heim et al., 2014). Additionally, dead needles are not considered to contribute to interception and the canopy is assumed to remain unchanged over the years. Therefore, damages from especially drought periods and hysteresis of soil water content after dry spells are not simulated in the model (Federer et al., 2003{Luong, 2022 #64)}. The hysteresis of the soil can be observed in Figure 5b and 8b, where the SWC scatter plot shows the characteristic s-shape due to delayed rewetting, which is not simulated by the model. The lacking changes would also explain the large overestimation of the ET rate by the model for 2019 by up to 28%, where the transpiration and productivity was still limited due to damages from the 2018 drought year (Lindroth et al., 2020). Similarly, other limiting factors cannot be considered here including nutrient and CO2 availability, which are generally more relevant on larger time scales, as well as inflow from streams or ground water.

Second, the separation of evaporation and transpiration can be difficult as it depends on the water availability, vegetation properties and soil properties (Federer, 1979). A study by

Baumgarten et al. (2014) showed that a version of the BROOK90 tends to overestimate transpiration at low soil moisture levels. However, it is difficult and often very costly to determine the transpiration rate experimentally, which is typically done by sap flow measurements on a few individual trees adding uncertainty by upscaling (Baumgarten et al., 2014). Therefore, even though the model makes assumptions regarding the soil and plant resistances to provide a parameterisation of the Shuttleworth and Wallace (1985) method, it provides a fast and cheap alternative, with relatively high accuracy to estimate transpiration (Baumgarten et al., 2014).

Third, the data used for the model validation come with uncertainties and inaccuracies as well. The measurement data was gap filled using the marginal distribution sampling (MDS) method, which approximates the atmospheric fluxes based on covariance with the meteorological drivers: air temperature, incoming shortwave radiation and vapour pressure deficit, as well as temporal autocorrelation (Mahabbati et al., 2021; Reichstein et al., 2005; Zhu et al., 2022). This method performs well compared to other approaches for short gaps but tends to increase in uncertainty with longer gaps. However, it is difficult to quantify the uncertainty as the methods performance and bias largely depends on the site properties (Reichstein et al., 2005). Inaccuracies from the gap filling method are displayed for the first few months of 2018, where data was missing for all variables leading to large differences between the model and the measurements. However, for the rest of the timeframe, the periods of missing data were typically a few hours to a few days leading to low inaccuracies connected to the gap filling method. Using the data with gaps was not an option here, as this study is comparing daily totals regarding the ET rate and gaps would create a large negative bias. The same goes for the gap filled input data from ICOS. Moving on, the short timeframe for the model validation with data from five full years (2018, 2019, 2021, 2022, 2023) might leave a bias since as shown in the results, those years are generally warmer with higher water stress compared to past years. Similarly, the choice of 2020 for tuning the model was arbitrary here and using a different year might have improved the model performance.

Lastly, the input data comes with uncertainty from sensor issues and biases from the measurement techniques. Especially precipitation measurements with precipitation gauges tend to show a negative bias (Dingman, 2015). Moreover, the temperature and wind speed data from Helsingborg A was arbitrarily adjusted to fit the data from Ljungbyhed using the slope of the linear relationship. However, given the spread of the data, this probably only improved the fit for part of the data, leading to worse result for other parts.

In the future it might be interesting to therefore adjust the SMHI data to fit the ICOS measurements, to possibly improve the model performance. Furthermore, applying the parameterized model to other sites and evaluating the performance might give insight into how sensitive the model is regarding its parameters. It would show, if the model can be applied to other forest sites without extensive parameter adjustments. Finally, applying a different, possibly less complex hydrological model to compare the accuracy could showcase the performance of BROOK90 for this type of ecosystem.

5.2 Water Balance at Hyltemossa since 1950

As shown in the results (Chapter 4.4), Hyltemossa experienced water stress periods as expected in the early 1950s, 1975 and 1976, 2018 and 2022 as well as in 1992 when assuming a fully grown forest stand. However, 1981-83; 1988-1989 and 2003 showed low to no water stress, while 1959, 1972, 2016 and 2020 displayed long dry periods (89 to 126 days) with low transpiration indices (0.79 to 0.9 on average), even though these years are typically not considered

as drought years in literature (Alavi, 2002; Hanel et al., 2018; Hänsel et al., 2022). This could be partly explained by the strong spatial variability of precipitation and regional differences. Particularly 2003 is a year that resulted in a drought for large parts of southern and central Europe, however, not as much in Scandinavia (Hänsel et al., 2022). Also, while the transpiration index can indicate stress to the plants, it does not directly reflect drought conditions. Most years with high water stress can be explained by variations in precipitation and temperature, with high water stress usually occurring in years with low precipitation and high maximum temperatures. This can be seen particularly in 1959 and 2018 with below average annual precipitation and above average maximum temperatures, resulting in the annual potential transpiration surpassing the precipitation. Furthermore, the inter annual variation in the transpiration index can be explained by the seasonal distribution of precipitation, with transpiration occurring mostly between spring and autumn. Therefore, even if a year shows high annual precipitation, the forest might still experience high water stress because of limited rain fall in the growing season, as shown in e.g., 1953. In this regard it is important to consider both duration and average annual transpiration index when evaluating the drought impact. As Allen et al. (2015) concludes, more intense and hotter droughts typically lead to higher mortality rates in forests. Nevertheless, this is dependent on the seasonal distribution of dry days, with trees showing the highest vulnerability during the growing season, which requires more detailed investigation of seasonal patterns here.

Overall, contrary to the hypothesis, the site shows no significant trend in annual precipitation or soil moisture and even though the annual ET would have increased significantly for a fully grown forest, the change is rather small with 0.85 mm/yr (around 0.1%). This is also accompanied by no significant increase in water stress or number of dry days. Given that this study concentrates on a singular location with large interannual variations in weather, the variations might drown out any significant trends. These might be more apparent on larger spatial scales, as described by Seneviratne (2023). However, a study by Ziche et al. (2021) for pine stands in Northern Germany also showed no significant change in precipitation or soil moisture between 1961 to 1990 and 1991 to 2019, with an increase of potential and actual evapotranspiration by about 6%, which is higher than modelled here. The difference in magnitude could be attributed to the difference in vegetation as well as location, with the pine forest displaying lower annual ET rates of around 480 mm, higher temperatures (around 8.5 °C annually) and lower precipitation (around 600 mm) as well as different soil properties. However, in both cases the increase in ET can most likely be attributed to the increase in temperature (here by about 1.1°C between 1950 to 1980 and 1981 to 2023). Moreover, studies by Ziche et al. (2021) and Meusburger et al. (2022) also identify 2018 to be a year with high drought impact with 2019 being also categorized as a drought year due to low winter precipitation leading to increased water deficit in the growing season. This was not captured well in the results here, possibly since the model cannot emulate drought damages from previous years, largely limiting the water uptake and transpiration rate.

The forest in Hyltemossa experienced exceptionally low water stress between 1980 and 2000 which can be attributed to the low canopy height and cover after the plantation in 1983 or 1988. This shows that planted forests experience largely reduced water scarcity during the first 15 to 20 years after plantation, again depending on the location and overall water input. However, this observation is largely dependent on the assumed change in LAI and height of the spruce forest. As described by Roloff et al. (2010), Norway spruce trees typically grow in a sigmoidal pattern with a slow growth at the age of up to 20 years, reaching the peak growth rate at the age of 40 years with exact growth rates depending largely on nutrient and water availability. However, for this thesis the growth was assumed to be linear with a rate of 3 meters in 5 years, which is considerably

higher than the average growth rate of 1 meter in 5 years measured by (Huuskonen et al., 2023; Kindermann et al., 2018; Weiner & Thomas, 2001; Zeide, 1993). But it might reflect the change in maximum tree height and is within the range of growth rates reported by Lee et al. (2024). Furthermore, the chosen coarse temporal resolution of 5 years per step does not allow for a detailed representation of the sigmoidal growth, which is additionally limited by the two stands that are lumped together having different ages and therefore different heights and LAI. Given that the forests were planted in 1983 and 1988 following clearcuts in 1982 and 1987, it is likely that the model underestimated the ET rate for 1980 to 1990. Likewise, the LAI and tree height are probably overestimated for 1990 to 2000 resulting in overestimated ET and AT rates for this period. Furthermore, the effect of thinning is here assumed to decrease the LAI by 30% between 2010 and 2015, although the forest was thinned twice in 2019 by 30% and 25% and again in 2013 by 15 % in one stand and by 30% in 2015 in the other stand, meaning that the impact of the thinning was most likely underestimated. This is difficult to evaluate since the exact relationship between LAI and stand density changes from thinning depend largely on the thinning technique and tree species and are largely understudied (Davi et al., 2008; Pokorný et al., 2008). Measurements on changes in LAI might be therefore of interest, also to represent the impact of management strategies more exactly.

Overall, the results' reliability here is largely limited by the accuracy of the input data, as mentioned before. The ET rate and most likely also the water stress is overestimated for most years at the site, as also shown when comparing the outputs with ICOS vs SMHI input data. The exact amount is difficult to evaluate, because of the large variation in precipitation between Hyltemossa and the SMHI station in Klippan and overall interannual variation in the input data. Furthermore, the vapour pressure and solar radiation data show large gaps, which were then interpolated by the model to typically potential values. Between 1950 and 1983 solar radiation data was unavailable, meaning that the model assumed a corrected potential insolation and therefore most likely overestimated the incoming shortwave radiation and ET rates. Moreover, since no information is provided on the vegetation cover or management before 1983, this period should be treated as a model for potential periods of water stress. Therefore, exact values should not be considered here, and the focus should be on general patterns between years.

5.3 Management and Climate change scenarios

Looking at the comparison of two different management approaches as well as the increasing temperatures regarding their impact on the water balance at Hyltemossa, one can see that higher stand density and temperature result in a significant increase in ET rate. The change in transpiration with temperature increase by 2°C is about 5% higher than with increased stand density. These scenarios also resulted, as expected, in a significant increase in water stress and number of dry days by around 29 and 11days respectively, prolonging the dry period by almost a month when assuming a uniform increase in temperature. Similarly, the ET rate, water stress and number of dry days is significantly reduced when introducing another thinning by 25%, shortening the dry period by about 23 days. This can be attributed to the water availability for the plants, where lower stand density with the same amount of incoming water leads to higher water availability for the individual trees, reducing the water stress with overall reduced potential transpiration rates (Alavi, 2002; Dingman, 2015). Meanwhile increasing temperature result in higher vapour pressure deficit in the air and higher potential transpiration rates. However, actual transpiration is limited by the availability of water, as sown for 2018. For that year differences in annual ET rate between the

scenarios is minor compared to other years because the actual transpiration is largely limited by precipitation input. This is lower than the potential transpiration for all scenarios in 2018. Accordingly, all scenarios exhibit similar transpiration rates with slightly different ET rates due to increased evaporation with higher stand density and temperatures. This results in overall interannual differences where the management strategies and climate change scenarios show lower changes for drought years regarding their ET rate and water stress. The number of dry days does not fully follow the same pattern.

Compared to other studies simulating the impact of climate change on the water balance of forest ecosystems, the results are generally similar. A study by Ziche et al. (2021) showed that under the RCP8.5 with an increase in temperature by about 2.6 to 3.6°C, there can be a linear increase in ET rate and PET expected with a significant increase in dry days for 2010 to 2100. Similarly, Tahir (2012) found that for both a temperate forest in Germany and a boreal forest in northern Sweden, the ET rate is expected to increase by around 40 and 30 mm/year respectively for 1°C increase in maximum temperatures. However, it should be noted that this study showed a relatively poor model performance, overestimating the ET rate at Norunda by up to 250%. Furthermore, these results are limited by the assumption that in the future the temperature would change equally for both maximum and minimum temperatures with no change in precipitation. However, as described by Seneviratne (2023), Sweden is projected to experience a slight increase in precipitation and temperature, with the exact increase depending on the forcing scenario and model applied. However, the projection for precipitation show high uncertainties and were therefore not considered in this thesis (Seneviratne, 2023). Furthermore, with climate change an increase in atmospheric carbon dioxide is projected to improve the water use efficiency of most forested ecosystems and studies disagree on whether this effect would counteract the increased drought damage from hotter droughts (Allen et al., 2015; Brodribb et al., 2020). This effect cannot be integrated into this hydrological model, given that it does not provide for parameters or input representing other limiting resources such as atmospheric carbon or nutrients, meaning that the water stress is most likely overestimated for the fourth scenario.

From the results one could infer that thinning can reduce the period of water stress each year by about 30 % with a reduction in ET rate by about 5% for each year, which was presented similarly by Tahir (2012), showing a decrease in ET rate by over 10% with a thinning of 30%. In contrast, a study by Boczoń et al. (2016) found that evapotranspiration and transpiration rate significantly increased after thinning in a pine stand. The study attributes this change to improved water use efficiency in the trees and higher ET in understory vegetation. This improved water use efficiency is also reflected in this thesis as modelled total annual transpiration is almost the same for the baseline and the thinning scenario in the drought year of 2018, meaning that individual trees transpire more under drought conditions after thinning. This in turn means that the damage to the individual trees is reduced substantially with still similar productivity levels. However, a study by Lagergren et al. (2008) showed that the impact of thinning on the transpiration rate of forests can differ significantly between years, with the difference in AT rate between the non-thinned and thinned stand diminishing over time from initially 40% to 20% in later years. Moreover, the thinned stand displayed up to 7 times higher transpiration rates during drought periods. This shows one of the limitations of the model which cannot emulate changes in the canopy including increasing LAI with the trees filling gaps left by thinning, as well as increased resilience in the forest. Therefore, studying the increase in LAI after thinning in the forest stand and adjusting the LAI parameter in the model would provide more insight into the actual physical process.

5.4 Suggested Improvements and potential future studies

As this study only focuses on one specific forest site in Sweden, the conclusion that can be drawn for forestry practices are very limited, therefore it might be of interest to apply the BROOK90 to multiple forested sites with the same vegetation to evaluate the differences between locations and produce a representative study for Swedish forests. Alternatively, applying the extension of BROOK90 in R for example, the global BROOK90 could provide a larger spatial cover and insight in specific variations of the water balance in regions of Sweden, even though it generally produces less reliable results than a calibrated lumped BROOK90 (Vorobevskii et al., 2022). Furthermore, the BROOK90-R introduced by (Kronenberg et al., 2019) can provide changes in parameters over time providing for vegetation growth. This could improve the model outputs for long time series, as applied here. Similarly, the LWF-BROOK90 introduced by (Schmidt-Walter et al., 2020) provides a soil parameterization, changes in the forest over time and with temperature, and could therefore improve the results. Furthermore, the result of this study could be used to evaluate other, possibly simpler hydrological models and their performance for modelling the water balance for a managed spruce stand.

6 Conclusion

In conclusion, the BROOK90 model provides robust and suitable model outputs to represent the water balance for the spruce forest at Hyltemossa. Although the model overestimates the evapotranspiration significantly when using input data from the closest meteorological stations, it still provides a good enough fit to model past water stress periods from 1950 onwards.

According to modelled transpiration index the forest experienced the highest water stress in 1951, 1959 and 2018 and drought periods in the early 1950s, 1964, 1972, 1975-76, 2016, 2020 and 2022. Even though there was a significant increase in temperature since 1950 as well as in evapotranspiration, the expected wetting trend was not shown in the precipitation or soil moisture data. Furthermore, the reported rise in temperatures also did not result in a significant increase in water stress or dry days per year.

The applied management and climate change scenarios showed a significant increase in water stress and evapotranspiration with an increase in temperature by 2°C or an increased stand density by 25%. In contrast a lowered stand density results in a significant reduction of evapotranspiration and dry days. This infers that further thinning could reduce the water stress in the spruce forest and therefore reduce the impact of future drought events.

Going forward, expanding the spatial extent of the model, and possibly applying the global BROOK90 could provide more insight into the water balance in the region Scania or the entirety of Sweden to study spatial variability of experienced water stress and impact of climate change on the water balance.

7 References

Literature

Abdollahi, K., Bazargan, A., & McKay, G. (2019). Water Balance Models in Environmental Modeling. In C. M. Hussain (Ed.), *Handbook of Environmental Materials Management*. https://doi.org/10.1007/978-3-319-58538-3_119-1

Alavi, G. (2002). The impact of soil moisture on stem growth of spruce forest during a 22-year period. *Forest Ecology and Management*, *166*(1), 17-33. https://doi.org/https://doi.org/10.1016/S0378-1127(01)00661-2

Allen, C. D., Breshears, D. D., & McDowell, N. G. (2015). On underestimation of global vulnerability to tree mortality and forest die-off from hotter drought in the Anthropocene. *Ecosphere*, *6*(8), art129. https://doi.org/https://doi.org/10.1890/ES15-00203.1

Baumgarten, M., Weis, W., Kühn, A., May, K., & Matyssek, R. (2014). Forest transpiration—targeted through xylem sap flux assessment versus hydrological modeling. *European Journal of Forest Research*, *133*(4), 677-690. https://doi.org/10.1007/s10342-014-0796-4

Belmonte, A., Sankey, T. T., Biederman, J., Bradford, J. B., & Kolb, T. (2022). Soil moisture response to seasonal drought conditions and post-thinning forest structure. *ECOHYDROLOGY*. https://doi.org/10.1002/eco.2406

Boczoń, A., M, D., & Kowalska, A. (2016). Effect of thinning on evaporation of Scots pine forest. *Applied Ecology and Environmental Research*, *14*, 367-379. https://doi.org/10.15666/aeer/1402_367379

Brodribb, T. J., Powers, J., Cochard, H., & Choat, B. (2020). Hanging by a thread? Forests and drought. *Science*, *368*(6488), 261-266. https://doi.org/doi:10.1126/science.aat7631

Buchtele, J., Herrmam, A., Maraga, F., & Bajracharya, O. R. (1998). Simulation of effects of land-use changes on runoff and evapotranspiration.*Iahs Publication* [Hydrology, water resources and ecology in headwaters]. HeadWater 98 Conference, Merano, Italy.

Chapin, F. S., Matson, P. A., Vitousek, P. M., & Chapin, M. C. (2011). *Principles of terrestrial ecosystem ecology*. Springer.

Chen, D., Zhang, P., Seftigen, K., Ou, T., Giese, M., & Barthel, R. (2021). Hydroclimate changes over Sweden in the twentieth and twenty-first centuries: a millennium perspective. *Geografiska Annaler: Series A, Physical Geography*, *103*(2), 103-131. https://doi.org/10.1080/04353676.2020.1841410

Clapp, R. B., & Hornberger, G. M. (1978). Empirical equations for some soil hydraulic properties. *Water Resources Research*, *14*(4), 601-604. https://doi.org/https://doi.org/10.1029/WR014i004p00601

Combalicer, E. A., Lee, S. H., Ahn, S., Kim, D. Y., & Im, S. (2008). Modeling Water Balance for the Small-Forested Watershed in Korea [Article]. *Ksce Journal of Civil Engineering*, *12*(5), 339-348. https://doi.org/10.1007/s12205-008-0339-y

Davi, H., Baret, F., Huc, R., & Dufrêne, E. (2008). Effect of thinning on LAI variance in heterogeneous forests. *Forest Ecology and Management*, *256*(5), 890-899. https://doi.org/https://doi.org/10.1016/j.foreco.2008.05.047

Dingman, S. L. (2015). *Physical hydrology*. Waveland Press.

Federer, C. A. (1979). A soil-plant-atmosphere model for transpiration and availability of soil water. *Water Resources Research*, *15*(3), 555-562. https://doi.org/https://doi.org/10.1029/WR015i003p00555

Federer, C. A. (1982). Transpirational supply and demand: Plant, soil, and atmospheric effects evaluated by simulation. *Water Resources Research*, *18*(2), 355-362. https://doi.org/https://doi.org/10.1029/WR018i002p00355

Federer, C. A. (Revised - April 9, 2021). *The BROOK90 Hydrologic Model - For Evaporation, Soil Water, and Streamflow*. Retrieved 08/05/2024 from http://www.ecoshift.net/brook/brook90.htm

Federer, C. A., Vörösmarty, C., & Fekete, B. (2003). Sensitivity of Annual Evaporation to Soil and Root Properties in Two Models of Contrasting Complexity. *Journal of Hydrometeorology*, *4*(6), 1276-1290. https://doi.org/https://doi.org/10.1175/1525-7541(2003)004<1276:SOAETS>2.0.CO;2

GustafsborgAB. (2016). *Utfölig Bestandslista, LandInfo Forest v 2.5*.

GustafsborgAB. (2024). *GUSTAFSBORGS SÄTERI AB*. Retrieved 23/05/2024 from https://gustafsborg.se/

Hammel, K., & Kennel, M. (2001). Charakterisierung und Analyse der Wasserverfügbarkeit und des Wasserhaushalts von Waldstandorten in Bayern mit dem Simulationsmodell BROOK90. In *Forstliche Forschungsberichte München* (Vol. 185). München: Frank. https://books.google.se/books?id=mAmItgAACAAJ

Hanel, M., Rakovec, O., Markonis, Y., Máca, P., Samaniego, L., Kyselý, J., & Kumar, R. (2018). Revisiting the recent European droughts from a long-term perspective. *Scientific Reports*, *8*(1), 9499. https://doi.org/10.1038/s41598-018-27464-4

Hänsel, S., Hoy, A., Brendel, C., & Maugeri, M. (2022). Record summers in Europe: Variations in drought and heavy precipitation during 1901–2018. *International Journal of Climatology*, *42*(12), 6235-6257. https://doi.org/https://doi.org/10.1002/joc.7587

Heim, A., Lundholm, J., & Philip, L. (2014). The impact of mosses on the growth of neighbouring vascular plants, substrate temperature and evapotranspiration on an extensive green roof. *Urban Ecosystems*, *17*(4), 1119-1133. https://doi.org/10.1007/s11252-014-0367-y

Heim, R. R. (2002). A Review of Twentieth-Century Drought Indices Used in the United States. *Bulletin of the American Meteorological Society*, *83*(8), 1149-1166. https://doi.org/https://doi.org/10.1175/1520-0477-83.8.1149

Holst, T., Rost, J., & Mayer, H. (2005). Net radiation balance for two forested slopes on opposite sides of a valley. *International Journal of Biometeorology*, *49*(5), 275-284. https://doi.org/10.1007/s00484-004-0251-1

Huuskonen, S., Lahtinen, T., Miina, J., Uotila, K., Bianchi, S., & Niemistö, P. (2023). Growth Dynamics of Young Mixed Norway Spruce and Birch Stands in Finland. *Forests*, *14*(1), 56. https://www.mdpi.com/1999-4907/14/1/56

ICOS. *Hyltemossa*. Retrieved 25/04/2024 from https://www.icos-sweden.se/hyltemossa

Kindermann, G. E., Kristöfel, F., Neumann, M., Rössler, G., Ledermann, T., & Schueler, S. (2018). 109 years of forest growth measurements from individual Norway spruce trees. *Scientific Data*, *5*(1), 180077. https://doi.org/10.1038/sdata.2018.77

Knutzen, F., Averbeck, P., Barrasso, C., Bouwer, L. M., Gardiner, B., Grünzweig, J. M., Hänel, S., Haustein, K., Johannessen, M. R., Kollet, S., Pietikaeinen, J. P., Pietras-Couffignal, K., Pinto, J. G., Rechid, D., Rousi, E., Russo, A., Suarez-Gutierrez, L., Wendler, J., Xoplaki, E., & Gliksman, D. (2023). Impacts and damages of the European multi-year drought and heat event 2018–2022 on forests, a review. *EGUsphere*, *2023*, 1-56. https://doi.org/10.5194/egusphere-2023-1463

Köppen, W. (1900). Versuch einer Klassifikation der Klimate, vorzugsweise nach ihren Beziehungen zur Pflanzenwelt.(Schluss). *Geographische Zeitschrift, 6*(12. H), 657-679.

Kronenberg, R., Güttler, T., Franke, J., & Bernhofer, C. (2013). Application of Synthetic Meteorological Time Series in BROOK90: A Case Study for the Tharandt Forest in Saxony, Germany. *Open Journal of Modern Hydrology, 3*, 214-225. https://doi.org/10.4236/ojmh.2013.34026

Kronenberg, R., Oehlschlägel, L., Bernhofer, C., & Luong, T. (2019). *Introducing an implementation of Brook90 in R*.

KSLA. (2015). *Forests and Forestry in Sweden*. https://www.skogsstyrelsen.se/globalassets/om-oss/rapporter/rapporter-20222021202020192018/rapport-2020-4-forest-management-in-sweden.pdf

Lagergren, F. (2001). *Effects of thinning, weather and soil moisture on tree and stand transpiration in a Swedish forest* [Theses]. Swedish Univ. of Agricultural Sciences (Sveriges lantbruksuniv. http://urn.kb.se/resolve?urn=urn:nbn:se:slu:epsilon-p-108002

Lagergren, F., Lankreijer, H., Kučera, J., Cienciala, E., Mölder, M., & Lindroth, A. (2008). Thinning effects on pine-spruce forest transpiration in central Sweden. *Forest Ecology and Management*, *255*(7), 2312-2323. https://doi.org/https://doi.org/10.1016/j.foreco.2007.12.047

Lee, D., Repola, J., Bianchi, S., Siipilehto, J., Lehtonen, M., Salminen, H., & Hynynen, J. (2024). Calibration models for diameter and height growth of Norway spruce growing in uneven-aged stands in Finland. *Forest Ecology and Management*, *558*, 121783. https://doi.org/https://doi.org/10.1016/j.foreco.2024.121783

Lee, J.-Y., Marotzke, J., Bala, G., Cao, L., Corti, S., Dunne, J. P., Engelbrecht, F., Fischer, E., Fyfe, J. C., Jones, C., Maycock, A., Mutemi, J., Ndiaye, O., Panickal, S., & Zhou, T. (2021). Future Global Climate: Scenario-based Projections and Near-term Information. In V. Masson-Delmotte, P. Zhai, A. Pirani, S. L. Connors, C. Péan, S. Berger, N. Caud, Y. Chen, L. Goldfarb, M. I. Gomis, M. Huang, K. Leitzell, E. Lonnoy, J. B. R. Matthews, T. K. Maycock, T. Waterfield, O. Yelekçi, R. Yu, & B. Zhou (Eds.), *Climate Change 2021 – The Physical Science Basis: Working Group I Contribution to the Sixth Assessment Report of the Intergovernmental Panel on Climate Change* (pp. 553-672). Cambridge University Press. https://doi.org/10.1017/9781009157896.006

Levin, I., Karstens, U., Eritt, M., Maier, F., Arnold, S., Rzesanke, D., Hammer, S., Ramonet, M., Vítková, G., Conil, S., Heliasz, M., Kubistin, D., & Lindauer, M. (2020). A dedicated flask sampling strategy developed for Integrated Carbon Observation System (ICOS) stations based on CO2 and CO measurements and Stochastic Time-Inverted Lagrangian Transport (STILT) footprint modelling. *Atmos. Chem. Phys.*, *20*(18), 11161-11180. https://doi.org/10.5194/acp-20-11161-2020

Lindroth, A., Holst, J., Linderson, M.-L., Aurela, M., Biermann, T., Heliasz, M., Chi, J., Ibrom, A., Kolari, P., Klemedtsson, L., Krasnova, A., Laurila, T., Lehner, I., Lohila, A., Mammarella, I., Mölder, M., Löfvenius, M. O., Peichl, M., Pilegaard, K., . . . Nilsson, M. (2020). Effects of drought and meteorological forcing on carbon and water fluxes in Nordic forests during the dry summer of 2018. *Philosophical Transactions of the Royal Society B: Biological Sciences, 375*(1810), 20190516. https://doi.org/doi:10.1098/rstb.2019.0516

Lloyd-Hughes, B., & Saunders, M. A. (2002). A drought climatology for Europe. *International Journal of Climatology, 22*(13), 1571-1592. https://doi.org/https://doi.org/10.1002/joc.846

Luong, T. T., Pöschmann, J., Kronenberg, R., & Bernhofer, C. (2021). Rainfall Threshold for Flash Flood Warning Based on Model Output of Soil Moisture: Case Study Wernersbach, Germany. *Water*, *13*(8), 1061. https://www.mdpi.com/2073-4441/13/8/1061

Luong, T. T., Pöschmann, J., Vorobevskii, I., Wiemann, S., Kronenberg, R., & Bernhofer, C. (2020). Pseudo-Spatially-Distributed Modeling of Water Balance Components in the Free State of Saxony. *Hydrology*, *7*(4), 84. https://www.mdpi.com/2306-5338/7/4/84

Luong, T. T., Vorobevskii, I., Pöschmann, J., Kronenberg, R., Gliksman, D., & Bernhofer, C. (2022). Evaluation of Long-Term Radar-Derived Precipitation for Water Balance Estimates: A Case Study for Multiple Catchments in Saxony, Germany. *Hydrology*, *9*(11), 204. https://www.mdpi.com/2306-5338/9/11/204

Mahabbati, A., Beringer, J., Leopold, M., McHugh, I., Cleverly, J., Isaac, P., & Izady, A. (2021). A comparison of gap-filling algorithms for eddy covariance fluxes and their drivers. *Geosci. Instrum. Method. Data Syst.*, *10*(1), 123-140. https://doi.org/10.5194/gi-10-123-2021

Mckee, T. B., Doesken, N. J., & Kleist, J. R. (1993). THE RELATIONSHIP OF DROUGHT FREQUENCY AND DURATION TO TIME SCALES.

Meusburger, K., Trotsiuk, V., Schmidt-Walter, P., Baltensweiler, A., Brun, P., Bernhard, F., Gharun, M., Habel, R., Hagedorn, F., Köchli, R., Psomas, A., Puhlmann, H., Thimonier, A., Waldner, P., Zimmermann, S., & Walthert, L. (2022). Soil–plant interactions modulated water availability of Swiss forests during the 2015 and 2018 droughts. *Global Change Biology*, *28*(20), 5928-5944. https://doi.org/https://doi.org/10.1111/gcb.16332

Monteith, J. L. (1965). Evaporation and environment. *Symp Soc Exp Biol*, *19*, 205-234.

Palmer, W. (2006). Meteorological Drought. Research Paper No. 45, 1965, 58 p. 1-65.

Pastorello, G., Trotta, C., Canfora, E., Chu, H., Christianson, D., Cheah, Y.-W., Poindexter, C., Chen, J., Elbashandy, A., Humphrey, M., Isaac, P., Polidori, D., Reichstein, M., Ribeca, A., van Ingen, C., Vuichard, N., Zhang, L., Amiro, B., Ammann, C., . . . Papale, D. (2020). The FLUXNET2015 dataset and the ONEFlux processing pipeline for eddy covariance data. *Scientific Data*, *7*(1), 225. https://doi.org/10.1038/s41597-020-0534-3

Pokorný, R., Tomášková, I., & Havránková, K. (2008). Temporal variation and efficiency of leaf area index in young mountain Norway spruce stand. *European Journal of Forest Research*, *127*(5), 359-367. https://doi.org/10.1007/s10342-008-0212-z

Pretzsch, H., Hilmers, T., Biber, P., Avdagić, A., Binder, F., Bončina, A., Bosela, M., Dobor, L., Forrester, D. I., Lévesque, M., Ibrahimspahić, A., Nagel, T. A., Río, M. d., Sitkova, Z., Schütze, G., Stajić, B., Stojanović, D., Uhl, E., Zlatanov, T., & Tognetti, R. (2020). Evidence of elevation-specific growth changes of spruce, fir, and beech in European mixed mountain forests during the last three centuries. *Canadian Journal of Forest Research*, *50*(7), 689-703. https://doi.org/10.1139/cjfr-2019-0368

Przybylski, T. (2007). Morphology. In M. G. Tjoelker, A. Boratyński, & W. Bugała (Eds.), *Biology and Ecology of Norway Spruce* (pp. 9-14). Springer Netherlands. https://doi.org/10.1007/978-1-4020-4841-8_2

Puhlmann, H., Schmidt-Walter, P., Hartmann, P., Meesenburg, H., & von Wilpert, K. (2019). Soil Water Budget and Drought Stress. In N. Wellbrock & A. Bolte (Eds.), *Status and Dynamics of Forests in Germany : Results of the National Forest Monitoring* (pp. 55-91). Springer International Publishing. https://doi.org/10.1007/978-3-030-15734-0_3

Reichstein, M., Falge, E., Baldocchi, D., Papale, D., Aubinet, M., Berbigier, P., Bernhofer, C., Buchmann, N., Gilmanov, T., Granier, A., Grünwald, T., Havránková, K., Ilvesniemi, H.,

Janous, D., Knohl, A., Laurila, T., Lohila, A., Loustau, D., Matteucci, G., . . . Valentini, R. (2005). On the separation of net ecosystem exchange into assimilation and ecosystem respiration: review and improved algorithm. *Global Change Biology*, *11*(9), 1424-1439. https://doi.org/https://doi.org/10.1111/j.1365-2486.2005.001002.x

Roberge, J.-M., Fries, C., Normark, E., Mårald, E., Sténs, A., Sandström, C., Sonesson, J., Appelqvist, C., & Lundmark, T. (2020). *Forest management in Sweden - Current practice and historical background*. Skogsstyrelsen. https://www.skogsstyrelsen.se/globalassets/om-oss/rapporter/rapporter-20222021202020192018/rapport-2020-4-forest-management-in-sweden.pdf

Roloff, A., H, W., U, L., & Stimm, B. (2010). *Bäume Mitteleuropas – Von Aspe bis Zirbel-Kiefer*.

Saksa, P. C., Conklin, M. H., Battles, J. J., Tague, C. L., & Bales, R. C. (2017). Forest thinning impacts on the water balance of Sierra Nevada mixed-conifer headwater basins. *Water Resources Research*, *53*(7), 5364-5381. https://doi.org/10.1002/2016WR019240

Salciccioli, J. D., Crutain, Y., Komorowski, M., & Marshall, D. C. (2016). Sensitivity Analysis and Model Validation. In M. I. T. C. Data (Ed.), *Secondary Analysis of Electronic Health Records* (pp. 263-271). Springer International Publishing. https://doi.org/10.1007/978-3-319-43742-2_17

Schmidt-Walter, P., Trotsiuk, V., Meusburger, K., Zacios, M., & Meesenburg, H. (2020). Advancing simulations of water fluxes, soil moisture and drought stress by using the LWF-Brook90 hydrological model in R. *Agricultural and Forest Meteorology*, *291*, 108023. https://doi.org/https://doi.org/10.1016/j.agrformet.2020.108023

Seneviratne, S. I., Nicholls, N., Easterling, D., Goodess, C. M., Kanae, S., Kossin, J., Luo, Y., Marengo, J., McInnes, K., Rahimi, M., Reichstein, M., Sorteberg, A., Vera, C., Zhang, X., Rusticucci, M., Semenov, V., Alexander, L. V., Allen, S., Benito, G., . . . Zwiers, F. W. (2012). Changes in Climate Extremes and their Impacts on the Natural Physical Environment. In C. B. Field, V. Barros, T. F. Stocker, & Q. Dahe (Eds.), *Managing the Risks of Extreme Events and Disasters to Advance Climate Change Adaptation: Special Report of the Intergovernmental Panel on Climate Change* (pp. 109-230). Cambridge University Press. https://doi.org/DOI: 10.1017/CBO9781139177245.006

Seneviratne, S. I., X. Zhang, M. Adnan, W. Badi, C. Dereczynski, A. Di Luca, S. Ghosh, I. Iskandar, J. Kossin, S. Lewis, F. Otto, I. Pinto, M. Satoh, S.M. Vicente-Serrano, M. Wehner, and B. Zhou. (2023). Weather and Climate Extreme Events in a Changing Climate. In C. Intergovernmental Panel on Climate (Ed.), *Climate Change 2021 – The Physical Science Basis: Working Group I Contribution to the Sixth Assessment Report of the Intergovernmental Panel on Climate Change* (pp. 1513-1766). Cambridge University Press. https://doi.org/DOI: 10.1017/9781009157896.013

SGU. (2024). Soil types 1:25000 - 1:100000. https://apps.sgu.se/kartvisare/kartvisare-jordarter-25-100.html

Shuttleworth, W. J., & Gurney, R. J. (1990). The theoretical relationship between foliage temperature and canopy resistance in sparse crops. *Quarterly Journal of the Royal Meteorological Society*, *116*(492), 497-519. https://doi.org/https://doi.org/10.1002/qj.49711649213

Shuttleworth, W. J., & Wallace, J. S. (1985). Evaporation from sparse crops-an energy combination theory. *Quarterly Journal of the Royal Meteorological Society*, *111*(469), 839-855. https://doi.org/https://doi.org/10.1002/qj.49711146910

SMHI. (2024). *Download meteorological observations* https://www.smhi.se/data/meteorologi/ladda-ner-meteorologiska-observationer#stations=core

Tahir, B. (2012). *Comparison of the water balance of two forest stands using the BROOK90 model* (Publication Number 255) Lund University]. Student thesis series INES (Dept of Physical Geography and Ecosystem Science). http://lup.lub.lu.se/student-papers/record/2861439

Trenberth, K. E., Dai, A., Rasmussen, R. M., & Parsons, D. B. (2003). The Changing Character of Precipitation. *Bulletin of the American Meteorological Society*, *84*(9), 1205-1218. https://doi.org/https://doi.org/10.1175/BAMS-84-9-1205

Trenberth, K. E., Dai, A., van der Schrier, G., Jones, P. D., Barichivich, J., Briffa, K. R., & Sheffield, J. (2014). Global warming and changes in drought. *Nature Climate Change*, *4*(1), 17-22. https://doi.org/10.1038/nclimate2067

Vicente-Serrano, S. M., Beguería, S., & López-Moreno, J. I. (2010). A Multiscalar Drought Index Sensitive to Global Warming: The Standardized Precipitation Evapotranspiration Index. *Journal of Climate*, *23*(7), 1696-1718. https://doi.org/https://doi.org/10.1175/2009JCLI2909.1

Vilhar, U., Starr, M., Katzensteiner, K., Simoncic, P., Kajfez-Bogataj, L., & Diaci, J. (2010). Modelling drainage fluxes in managed and natural forests in the Dinaric karst: a model comparison study [Article]. *European Journal of Forest Research*, *129*(4), 729-740. https://doi.org/10.1007/s10342-010-0379-y

Vorobevskii, I. (2022). *Modelling the water balance in small catchments: Development of a global application for a local scale*

Vorobevskii, I., Luong, T. T., Kronenberg, R., Grünwald, T., & Bernhofer, C. (2022). Modelling evaporation with local, regional and global BROOK90 frameworks: importance of parameterization and forcing. *Hydrol. Earth Syst. Sci.*, *26*(12), 3177-3239. https://doi.org/10.5194/hess-26-3177-2022

Vuichard, N., & Papale, D. (2015). Filling the gaps in meteorological continuous data measured at FLUXNET sites with ERA-Interim reanalysis. *Earth Syst. Sci. Data*, *7*(2), 157-171. https://doi.org/10.5194/essd-7-157-2015

Wang, K., Dickinson, R. E., & Ma, Q. (2020). Chapter 18 - Terrestrial evapotranspiration. In S. Liang & J. Wang (Eds.), *Advanced Remote Sensing (Second Edition)* (pp. 649-684). Academic Press. https://doi.org/https://doi.org/10.1016/B978-0-12-815826-5.00017-9

Weiner, J., & Thomas, S. C. (2001). The Nature of Tree Growth and the "Age-Related Decline in Forest Productivity". *Oikos*, *94*(2), 374-376. http://www.jstor.org/stable/3547583

Wellpott, A., Imbery, F., Schindler, D., & Mayer, H. (2005). Simulation of drought for a Scots pine forest (Pinus sylvestris L.) in the southern upper Rhine plain. *Meteorologische Zeitschrift*, *14*(2), 143-150. https://doi.org/10.1127/0941-2948/2005/0015

Zanchi, G., Belyazid, S., Akselsson, C., & Yu, L. (2014). Modelling the effects of management intensification on multiple forest services: a Swedish case study. *Ecological Modelling BECC: Biodiversity and Ecosystem services in a Changing Climate*, *284*, 48-59. https://doi.org/10.1016/j.ecolmodel.2014.04.006

Zeide, B. (1993). Analysis of Growth Equations. *Forest Science*, *39*(3), 594-616. https://doi.org/10.1093/forestscience/39.3.594

Zheng, W., Lamačová, A., Yu, X., Krám, P., Hruška, J., Zahradníček, P., Štěpánek, P., & Farda, A. (2021). Assess hydrological responses to a warming climate at the Lysina Critical Zone

Observatory in Central Europe. *Hydrological Processes*, *35*(9), e14281. https://doi.org/https://doi.org/10.1002/hyp.14281

Zhu, S., Clement, R., McCalmont, J., Davies, C. A., & Hill, T. (2022). Stable gap-filling for longer eddy covariance data gaps: A globally validated machine-learning approach for carbon dioxide, water, and energy fluxes. *Agricultural and Forest Meteorology*, *314*, 108777. https://doi.org/https://doi.org/10.1016/j.agrformet.2021.108777

Ziche, D., Riek, W., Russ, A., Hentschel, R., & Martin, J. (2021). Water Budgets of Managed Forests in Northeast Germany under Climate Change—Results from a Model Study on Forest Monitoring Sites. *Applied Sciences*, *11*(5), 2403. https://www.mdpi.com/2076-3417/11/5/2403

Data

Heliasz, M., Kljun, N., Biermann, T., Holst, J., Holst, T., Linderson, M.-L., Mölder, M., & Rinne, J. (2024). *ETC L2 Fluxnet (half-hourly), Hyltemossa, 2017-12-31–2023-12-31*. https://hdl.handle.net/11676/iG-rvKqvWOP3CxO7RInQzHkG

Heliasz, M., Kljun, N., Biermann, T., Holst, J., Holst, T., Linderson, M.-L., Mölder, M., Rinne, J., & Easterling, D. (2024). *ETC L2 Fluxes, Hyltemossa, 2017-12-31–2023-12-31* ICOS RI. https://hdl.handle.net/11676/XESY-JxtNIMxXKat66tMUD9y

Heliasz, M., Mölder, M., Kljun, N., Biermann, T., Holst, J., Holst, T., Linderson, M.-L., & Rinne, J. (2024). *ETC L2 ARCHIVE, Hyltemossa, 2017-12-31–2023-12-31* ICOS RI. https://hdl.handle.net/11676/BgNA1zoReXgZfAUPj6nInXNs

HelsingborgA. (2024a). *Mean_Temp_HelsingborgA_1995_2024* SMHI Stationnetwrok (62040). https://www.smhi.se/data/meteorologi/ladda-ner-meteorologiska-observationer#stations=core,param=airHumidity,stationid=63050

HelsingborgA. (2024b). *RH_HelsingborgA_1995_2024* SMHI Stationnetwrok (62040). https://www.smhi.se/data/meteorologi/ladda-ner-meteorologiska-observationer#stations=core,param=airHumidity,stationid=63050

HelsingborgA. (2024c). *Temp_HelsingborgA_1995_2024* SMHI Stationnetwrok (62040). https://www.smhi.se/data/meteorologi/ladda-ner-meteorologiska-observationer#stations=core,param=airHumidity,stationid=63050

HelsingborgA. (2024d). *Wind_HelsingborgA_1995_2024* SMHI Stationnetwrok (62040). https://www.smhi.se/data/meteorologi/ladda-ner-meteorologiska-observationer#stations=core,param=airHumidity,stationid=63050

Klippan. (2024). *Precip_Klippan_1945_2024* SMHI Stationnetwrok (63070). https://www.smhi.se/data/meteorologi/ladda-ner-meteorologiska-observationer#stations=core,param=airHumidity,stationid=63050

LjungbyA. (2024). *Mean_Temp_Ljungbyhet_1961_2008* SMHI Stationnetwrok (63510). https://www.smhi.se/data/meteorologi/ladda-ner-meteorologiska-observationer#stations=core,param=airHumidity,stationid=63050

Ljungbyhed. (2024a). *RH_Ljungbyhed_1951_2000* SMHI Stationnetwrok (63050). https://www.smhi.se/data/meteorologi/ladda-ner-meteorologiska-observationer#stations=core,param=airHumidity,stationid=63050

Ljungbyhed. (2024b). *Temp_min_max_Ljungbyhed_1951_2001* SMHI Stationnetwrok (63050). https://www.smhi.se/data/meteorologi/ladda-ner-meteorologiska-observationer#stations=core,param=airHumidity,stationid=63050

Ljungbyhed. (2024c). *Wind_Ljungbyhed_1939_2001* SMHI Stationnetwrok (63050). https://www.smhi.se/data/meteorologi/ladda-ner-meteorologiska-observationer#stations=core,param=airHumidity,stationid=63050

LundSol. (2024). *Radiation_LundSol_1983_2024* SMHI Stationnetwrok (53445). https://www.smhi.se/data/meteorologi/ladda-ner-meteorologiska-observationer#stations=core,param=airHumidity,stationid=63050

Software

Federer, C. A. (2002). BROOK 90: A simulation model for evaporation, soil water, and streamflow. In: http://www.ecoshift.net/brook/brook90.htm.

Federer, C. A. (2019). *BROOK90 for Windows*. In (Version 4.8a) C. Anthony Federer. http://www.ecoshift.net/brook/brook90.html

8 Appendix

Appendix 1: All Parameters used in BROOK90 sorted by their parameter file (Location, Flow, Canopy, Soil, Fixed and Initial) after calibrating to measured Evapotranspiration rate and Soil Water Content at Hyltemossa in 2020. All parameters including abbreviations, units, physical meaning and value ranges are explained in detail by Federer (2002). Parameters that are marked green include information and help within the model interaction surface (Federer, 2019). GW stands for ground water.

File	Parameter (Abbreviation)	Set Value					Tested values
Flow	Infiltration Depth (IDEPTH) in mm	500					750, 730, 1000
	Impermeable fraction (IMPERV)	0.2					0, 0.02, 0.05, 0.3
	Infiltration distribution (INFEXP)	1					0, 0.5, 0.75
	Binary Bypass flow variable (BYPAR)	0 = “no bypass flow”					-
	Bypass flow depth (QDEPTH) in mm	0					500, 730
	(QFPAR) – ignored since BYPAR = 0	0.2					
	(QFFC) – ignored since BYPAR = 0	0.3					
	Slope length from ridge to channel (LENGTH) in m	100					Ignored since DSLOPE = 0
	Hillside slope allowing matric flow (DSLOPE) in °	0					-
	Fractional multiplier for flow from lowest soil layer to GW (DRAIN)	1					-
	GW storage going to GW flow and Seepage (GSC), fraction	0					-
	GW discharge going to Seepage (GSP), fraction	0					-
Soil	Layer Thickness (THICK) in mm	40	35	125	450	700	All 100
	Field Capacity Ψ (PSIF) in kPa	-10	-8	-10	-12	-8.5	-5.5, -8.5, -10.0

	Field Capacity Θ (THETAF)	0.39	0.4	0.39	0.4	0.39	0.2, 0.32, 0.37, 0.4
	Brooks exponent (BEXP)	5.39	6	5.5	3.5	4	3, 3.5, 4, 5.5, 6, 7
	Hydraulic Conductivity (KF) in mm/d	6.3	5	7	6.5	5	1, 3, 5, 6.3, 7, 10
	Stone Content (STONEF)	0	0	0	0	0.5	0.1, 0.2, 0.3, 0.5
	Gravity potential in middle of soil layer (PSIG) in kPa	All 0.92					-
	Number of soil layers (NLAYER)	5					-
Canopy	Albedo (ALB)	0.09					-
	Albedo with snow on ground (ALBSN), fraction	0.14					-
	Reduction factor for snow evaporation (KSNVP), fraction	0.3					-
	Roughness factor of ground below canopy (Z0G), m	0.02					-
	Ratio of projected stem area index to height (CS)	0.035					-
	Total root length at maximum seasonal canopy height (MXRTLN), m/m²	2100					-
	Critical leaf water potential for stomata closure (PSICR), MPa	-2					-
	Average leaf width (LWIDTH), m	0.004					-
	Solar radiation extinction coefficient (CR), f	0.5					-
	TL, °C	0					Temperatures ranges for influence on leaf conductance – no change between T1 and T2; limited outside TL to TH
	T1, °C	10					
	T2, °C	30					
	TH, °C	40					

	Maximum height (MAXHT) in m	24.4	-
	Maximum LAI (MAXLAI)	5	AVG up to 4.92
	Internal Conductivity (MXKPL) in mm/day,MPa	8	2, 3, 4, 5, 8,
	Internal plant resistance (FXYLEM)	0.5	0.1, 0.6, 0.9
	Max Leaf Conductance (GLMAX) in cm/s	0.53	0.2, 0.3, 0.4, 0.6
	Root density (ROOTDEN) per 100 mm soil layer (f)	0.44, 0.25, 0.14, 0.08, 0.04, 0.02, 0.01, 0	-
Location	Latitude (LAT) in °N	56.1°N	-
	Slope (ESLOPE), °	2.0	-
	Slope Aspect (ASPECT), °CW	270	-
	Base temperature separating snow and rain (RSTEMP), °C	-0.5	-
	Degree-day snowmelt factor (MELFAC), MJ/(m²,day,K)	1.5	-
	Variation of LAI (RELLAI) (at day: 1, 54, 84, 299, 329, 366)	0, 0.5, 1, 1, 0.5, 0	1 (all year)
	Average Daily Precipitation Duration per month (DURATION) in h/day	4,3,3,2,2,2,2,2,2,3,3,4	-
	Fraction varying canopy height throughout year (RELHT)	1 (all year)	-

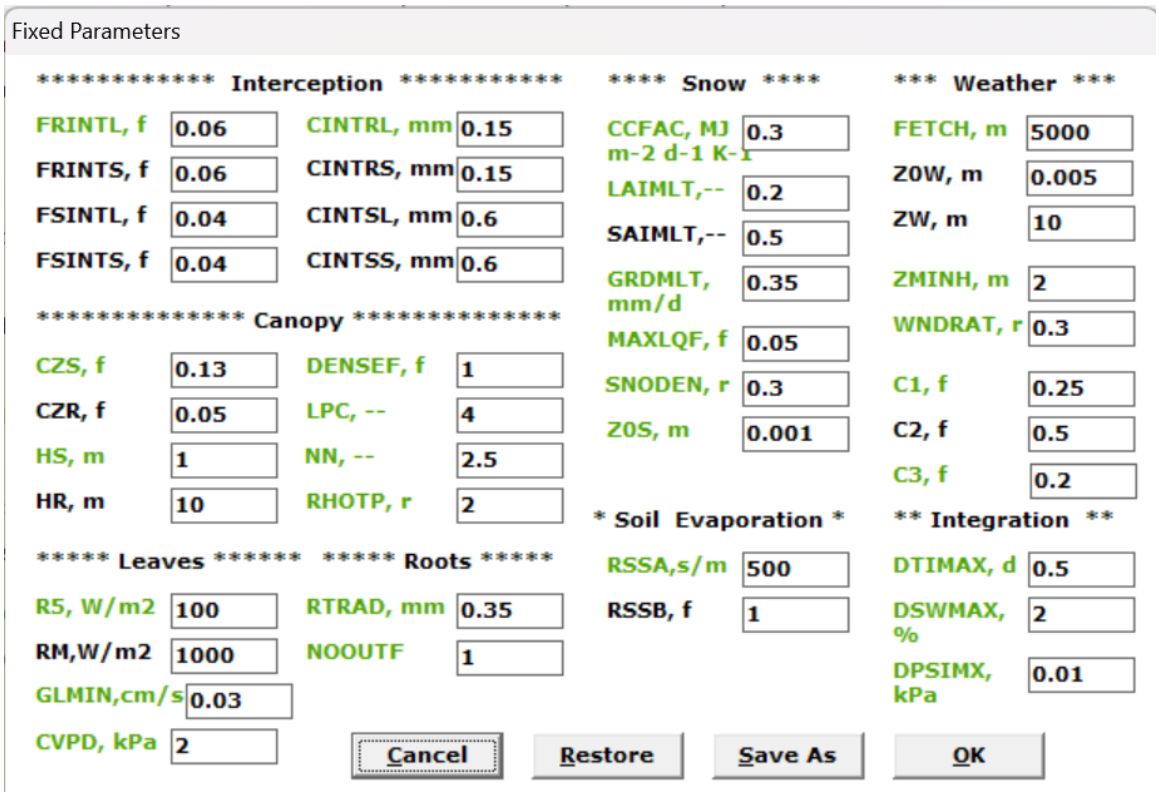
Fixed Parameters
********** Interception **********
FRINTL, f 0.06
FRINTS, f 0.06
FSINTL, f 0.04
FSINTS, f 0.04
CINTRL, mm 0.15
CINTRS, mm 0.15
CINTSL, mm 0.6
CINTSS, mm 0.6
********** Canopy **********
CZS, f 0.13
CZR, f 0.05
HS, m 1
HR, m 10
DENSEF, f 1
LPC, -- 4
NN, -- 2.5
RHOTP, r 2
***** Leaves ******
R5, W/m2 100
RM,W/m2 1000
GLMIN,cm/s 0.03
CVPD, kPa 2
***** Roots *****
RTRAD, mm 0.35
NOOUTF 1
**** Snow ****
CCFAC, MJ m-2 d-1 K-1 0.3
LAIMLT,-- 0.2
SAIMLT,-- 0.5
GRDMLT, mm/d 0.35
MAXLQF, f 0.05
SNODEN, r 0.3
Z0S, m 0.001
* Soil Evaporation *
RSSA,s/m 500
RSSB, f 1
*** Weather ***
FETCH, m 5000
Z0W, m 0.005
ZW, m 10
ZMINH, m 2
WNDRAT, r 0.3
C1, f 0.25
C2, f 0.5
C3, f 0.2
** Integration **
DTIMAX, d 0.5
DSWMAX, % 2
DPSIMX, kPa 0.01
Cancel
Restore
Save As
OK

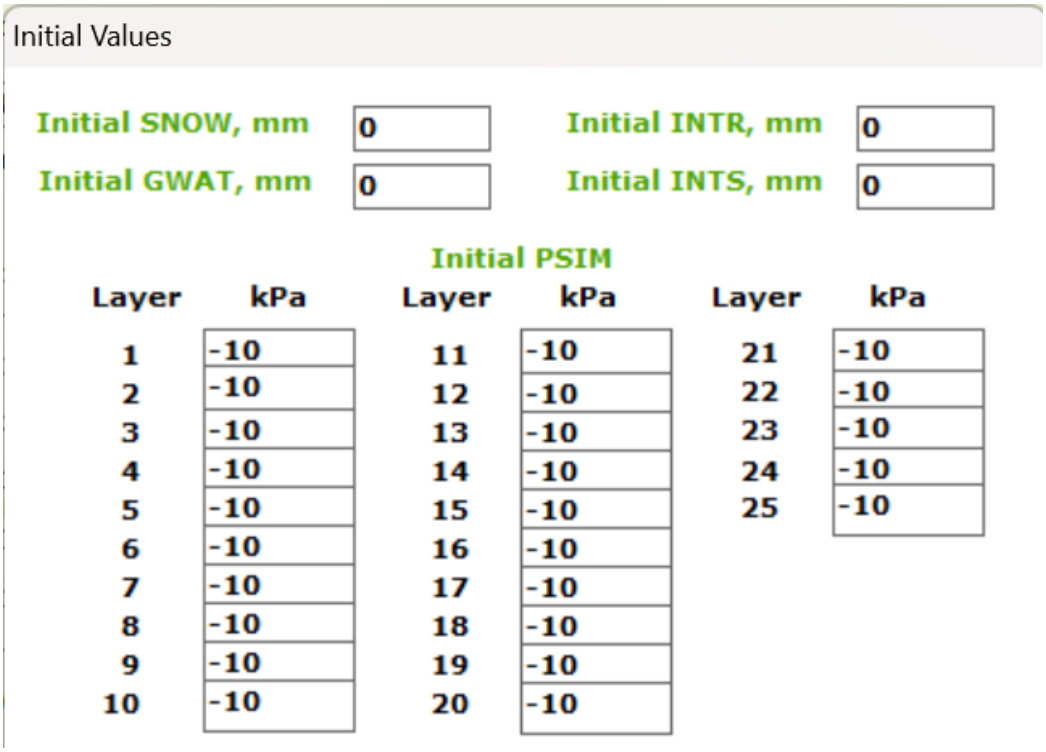
Initial Values
Initial SNOW, mm 0
Initial INTR, mm 0
Initial GWAT, mm 0
Initial INTS, mm 0
Initial PSIM
Layer kPa Layer kPa Layer kPa
1 -10
2 -10
3 -10
4 -10
5 -10
6 -10
7 -10
8 -10
9 -10
10 -10
11 -10
12 -10
13 -10
14 -10
15 -10
16 -10
17 -10
18 -10
19 -10
20 -10
21 -10
22 -10
23 -10
24 -10
25 -10

Appendix 2: Measured and Modelled Volumetric Soil Water Content (SWC) in the first soil layer (1) after parameterizing BROOK90 for Hyltemossa in 2020.

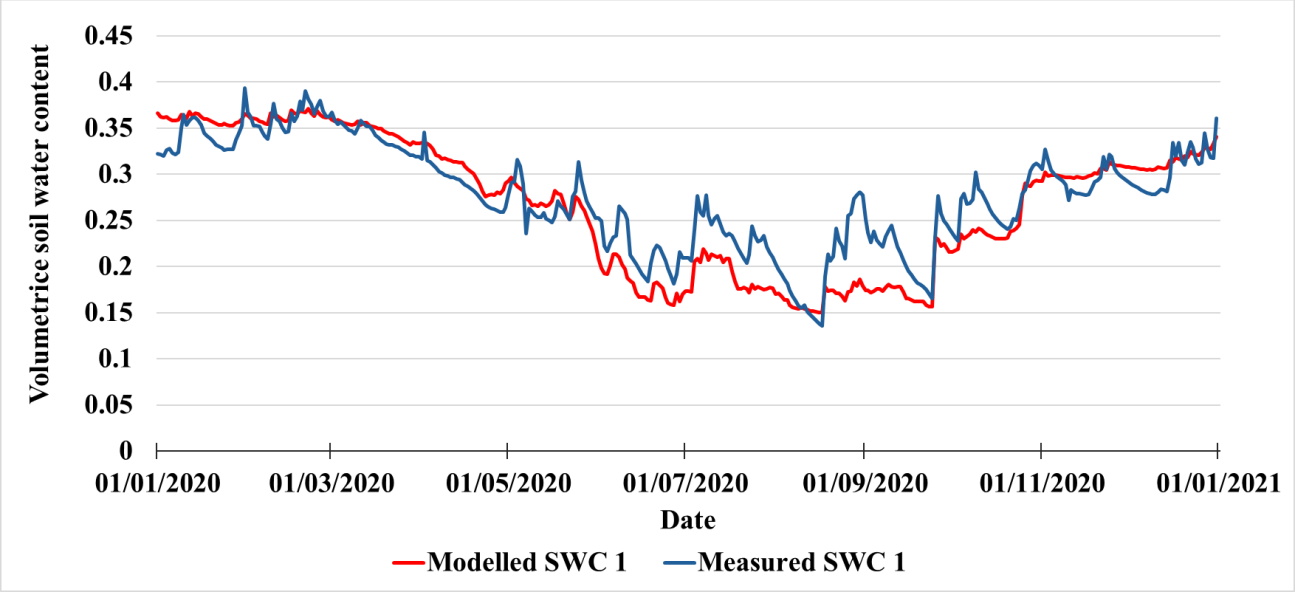

Appendix 3: Regression analysis comparing measured and modelled volumetric soil water content (SWC) for the second, third, fourth and fifth soil layer (a) to d) - 2 to 5) at Hyltemossa for 2020. This includes the linear regression slope (y) and R².

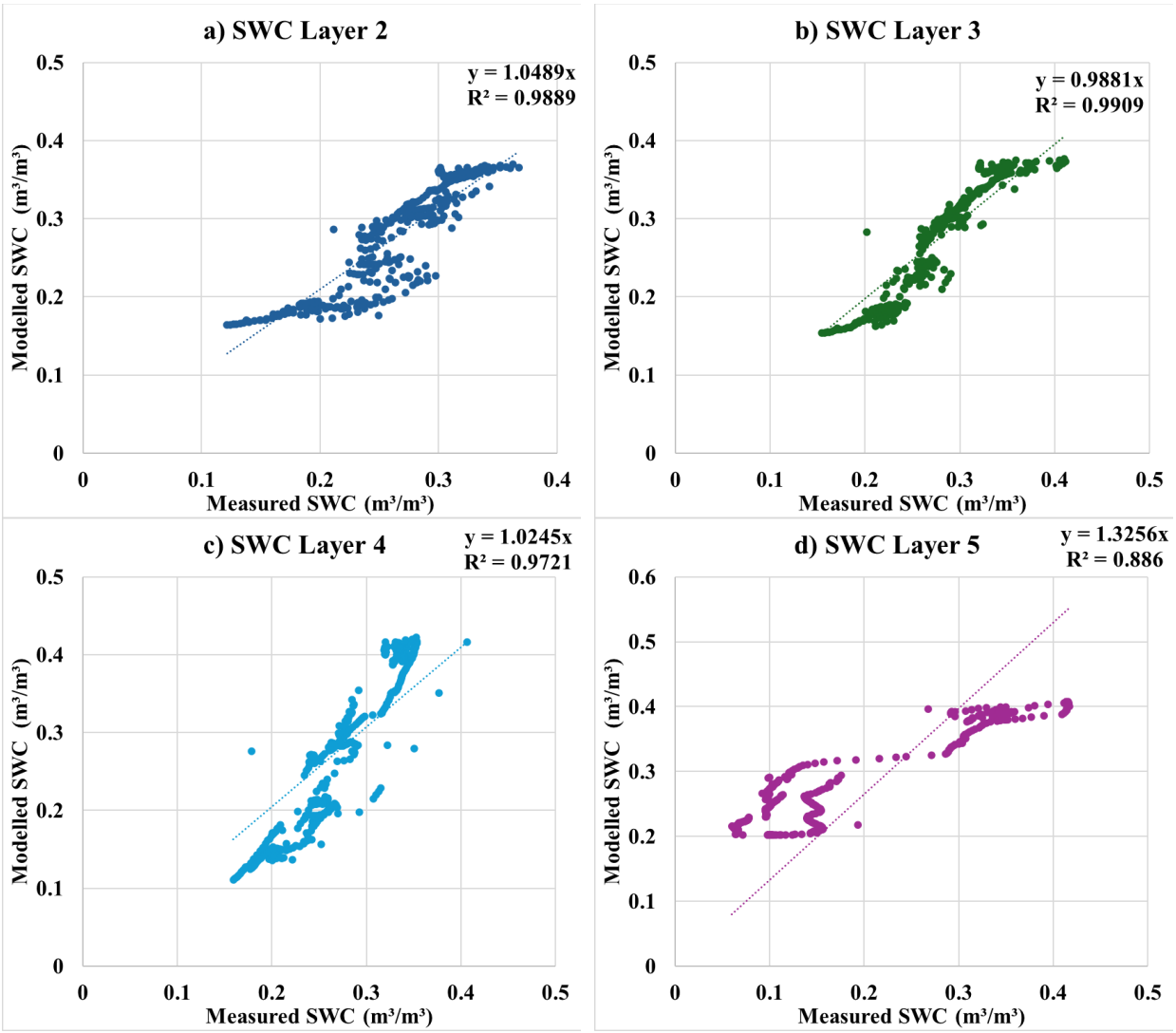

Appendix 4: Comparison of measured (blue) and modelled Total Soil Water Content through all layers (SWAT, in mm) using different input data sets (from SMHI stations in black and ICOS in red) for 2018 to the end of 2022 at Hyltemossa.

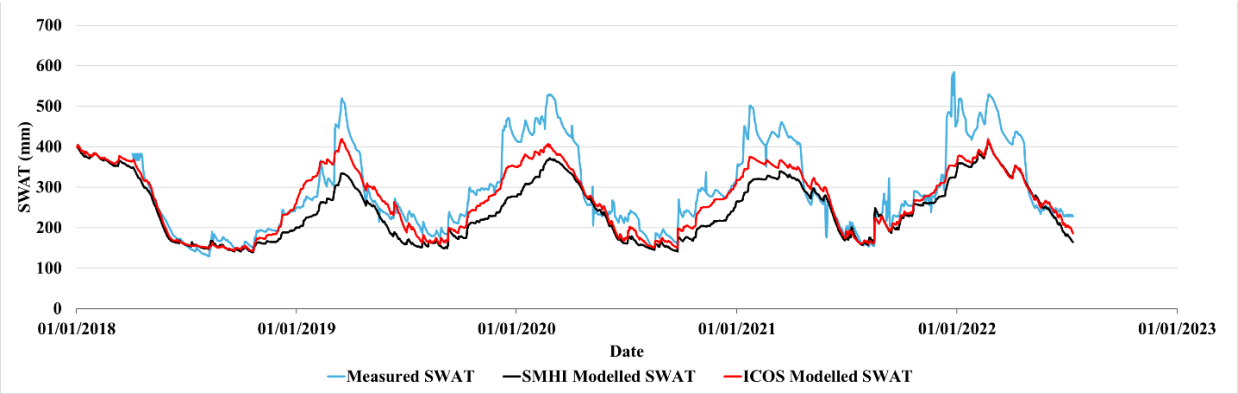

Appendix 5: Modelled daily evapotranspiration and transpiration rate at Hyltemossa for 1950 to 2023 based on SMHI input data assuming a changing leaf area index and tree height over time.

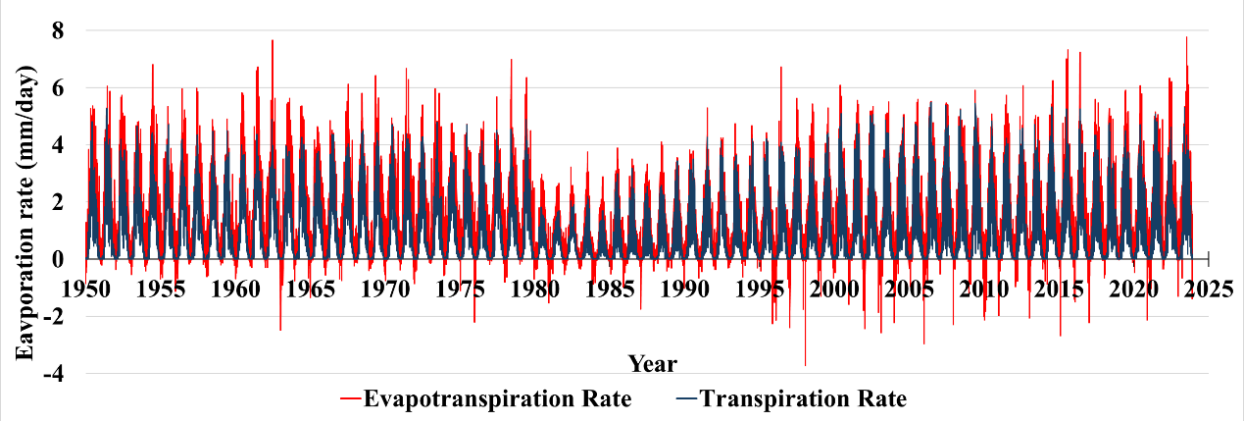

Appendix 6: Potential Evapotranspiration and transpiration rates at Hyltemossa, assuming and unchanging forest stand with a maximum LAI (MAXLAI) of 5 and maximum tree height of 27 m.